NASA TECHNICAL REPORT

NASA TR R-238

c. 1

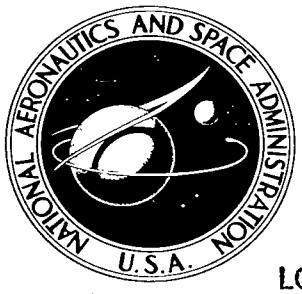

NASA TR R-238

THE DISPLACEMENTS IN AN ELASTIC HALF-SPACE DUE TO A MOVING CONCENTRATED NORMAL LOAD

by Donald L. Lansing

Langley Research Center
Langley Station, Hampton, Va.

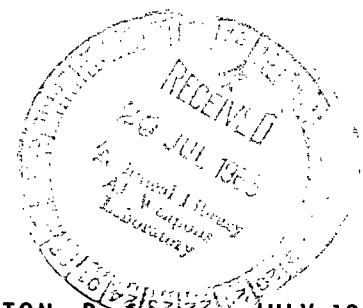

NATIONAL AERONAUTICS AND SPACE ADMINISTRATION • WASHINGTON, D. C. • JULY 1966

NASA TR R-238

THE DISPLACEMENTS IN AN ELASTIC HALF-SPACE DUE TO A MOVING CONCENTRATED NORMAL LOAD

By Donald L. Lansing

Langley Research Center
Langley Station, Hampton, Va.

NATIONAL AERONAUTICS AND SPACE ADMINISTRATION

For sale by the Clearinghouse for Federal Scientific and Technical Information
Springfield, Virginia 22151 – Price $3.00

CONTENTS

THE DISPLACEMENTS IN AN ELASTIC HALF-SPACE DUE TO A MOVING CONCENTRATED NORMAL LOAD

By Donald L. Lansing
Langley Research Center

SUMMARY

Equations are derived for the steady-state displacements produced at any point within an elastic half-space by a concentrated normal load in uniform motion over the surface. The results are valid for all depths, load speeds, and elastic constants. The equations for the displacements produced on the surface and in the vertical plane containing the line of motion of the load for the special case of Poisson's ratio equal to 1/4 are obtained from the general results and are expressed in terms of elementary functions and elliptic integrals. Some numerical calculations based upon these equations are presented and discussed for a wide range of load speeds. In addition, the complete time-dependent equations for the horizontal displacements produced at the surface, including the transients excited by the initial application of the load, are derived.

INTRODUCTION

Supersonic aircraft, air bomb bursts, and surface vehicles produce forces which act upon and move over the earth's surface. As a result of the earth's elasticity, these loads are transmitted through the earth's outer layers and over the ground surface and thereby produce disturbances at some distance from the area directly in contact with the load. These disturbances can set off a buried mine, can shake building occupants, and, if sufficiently severe, can produce damage to structures. The practical need for estimating the magnitudes of the ground motions and stresses induced by moving surface loads as well as the interesting theoretical aspects of the problem has produced over the past few years a number of papers on the fundamental dynamic phenomena involved. (See refs. 1 to 5.)

In order to investigate the displacements and stresses produced in the earth by a moving surface load by using the classical linear theory of elasticity, it is necessary to idealize the actual situation to some extent. A convenient starting point to the problem of calculating these disturbances is to assume that they are produced on a uniform semi-infinite elastic half space by a concentrated normal surface load moving in a straight line at constant speed. No generality is lost in assuming a concentrated load since more

general load distributions may then be built up by familiar superposition principles. The assumptions of a uniform medium with a plane surface and rectilinear motion limit the usefulness of the results but these conditions are fulfilled, or nearly so, in some practical problems and are sufficient for gaining an insight into the basic phenomena to be expected in more realistic situations.

A theoretical analysis of even this simplified problem is made difficult, and challenging, by the fact that there are three fundamental wave speeds in an elastic half-space. In decreasing order of magnitude, these speeds are the speeds of propagation of longitudinal waves, shear waves, and surface waves. The solution takes different forms and the details of an analysis vary depending upon the speed of the load relative to these three wave speeds. In this paper the load speed is referred to as "subseismic," "superseismic," and "transeismic" when it is less than the shear wave speed, greater than the longitudinal wave speed, and intermediate between these two speeds. Furthermore, one may decide to treat the complete time-dependent problem and account for the starting transients excited by the initial application of the load or, in the interests of further simplicity, one may treat just the steady-state case and obtain a description valid only after the load has been moving for some time. These factors and other considerations lead to a wide variety of partial problems which are gradually being solved piecemeal as the need for further information and theoretical interest in the basic problem develops.

The two-dimensional moving-line load was treated in the steady-state case in reference 1 at subseismic speeds and in reference 2 where the displacements and stresses were derived for all load speeds. These results were extended at subseismic speeds in reference 3 to include in the stresses the transient effects excited by the initial application of the line load. The steady-state displacements produced by a moving-point load at low subseismic speeds were derived in reference 4. The transient solution for the surface displacements was treated at all load speeds in reference 5. No work appears to be available on the subsurface stresses produced by the moving-point load.

The present paper is a continuation of the study of the three-dimensional case. Two aspects of this problem are considered. First, equations are derived for the steady-state displacements produced within an elastic half-space by a concentrated normal load moving at constant speed in a straight line over the surface. The results, obtained by Fourier transform methods, are valid for any depth, load speed, or elastic constants and could be used for an evaluation of the subsurface stresses and strains. The general equations for the displacements, which are in the form of double integrals with infinite limits, are then reduced to single integrals with finite limits. It is further shown that in the special case for Poisson's ratio equal to 1/4, the surface displacements can be expressed in terms of elementary functions and elliptic integrals. Some numerical calculations of the steady-state displacements at the surface and in the

vertical plane containing the line of motion of the load are presented and discussed. Second, equations are derived for the horizontal surface displacements which include the transients excited by the initial application of the load. These results, obtained by superimposing the response of the surface to an impulse, can also be expressed in terms of elliptic integrals and contain the steady-state solution at the surface as a special limiting case.

SYMBOLS

a,b,c — variables

$A(\theta),B(\theta),C(\theta),D(\theta)$ — quantities defined in equation (46)

$B_l = \sqrt{1 - M_l^2}$

$B_t = \sqrt{1 - M_t^2}$

c_l — velocity of longitudinal compression waves, $\sqrt{\frac{\lambda' + 2\mu'}{\rho_o}}$

c_R — velocity of Rayleigh waves

c_t — velocity of transverse shear waves, $\sqrt{\frac{\mu'}{\rho_o}}$

$$C^+(a,b,c) = \frac{a}{a^2 + (b - c)^2} + \frac{a}{a^2 + (b + c)^2}$$

$$C^-(a,b,c) = \frac{a}{a^2 + (b - c)^2} - \frac{a}{a^2 + (b + c)^2}$$

f,g — functions

$H(x)$ — unit step function, +1 when $x > 0$ and 0 when $x < 0$

$i = \sqrt{-1}$

k modulus of elliptic integrals

$K(k)$ complete elliptic integral of the first kind, $\int_0^{\pi/2} \frac{d\theta}{\sqrt{1 - k^2 \sin^2 \theta}}$

$M_l = \frac{V}{c_l}$

$M_R = \frac{V}{c_R}$

$M_t = \frac{V}{c_t}$

$N_1(\psi), N_2(\psi)$ quantities defined in equations (61) and (62)

P magnitude of concentrated load

$P' = \frac{P}{\mu'}$

$\left.\begin{matrix} r, \theta \\ \bar{r}, \varphi \end{matrix}\right\}$ polar coordinates

R_δ radial displacement produced on surface by an impulse

$R(\tau) = \frac{\mu' r^2}{c_t} R_\delta$

$S_l = \sqrt{\lambda^2 + \mu^2 - \lambda^2 M_l^2 - iV\epsilon\lambda}$

$S_t = \sqrt{\lambda^2 + \mu^2 - \lambda^2 M_t^2 - iV\epsilon\lambda}$

$S^+(a,b,c) = \frac{b - c}{a^2 + (b - c)^2} + \frac{b + c}{a^2 + (b + c)^2}$

$\operatorname{sgn}(x)$ sign function, $\frac{x}{|x|}$

t — time

$T(\varphi) = \left(1 - \frac{1}{4} M_t^2 \sin^2\varphi\right)\left(1 - \alpha_1^2 M_t^2 \sin^2\varphi\right)\left(1 - \alpha_2^2 M_t^2 \sin^2\varphi\right)$

$T(\bar{x},y) = \left(\bar{r}^2 - \frac{1}{4} M_t^2 y^2\right)\left(\bar{r}^2 - \alpha_1^2 M_t^2 y^2\right)\left(\bar{r}^2 - \alpha_2^2 M_t^2 y^2\right)$

u,v,w — Cartesian components of displacements

u',v',w' — contribution of Rayleigh poles to displacements (see eqs. (27) and (49))

u'',v'',w'' — integrals in displacements (see eqs. (27) to (47))

u_1, u_2, u_3
v_1, v_2, v_3
w_1, w_2, w_3 — quantities defined in equations (37) to (45)

$u_{\bar{r}}, u_\varphi$ — polar components of steady-state surface displacements

u_r, u_θ — polar components of transient surface displacements

$u_{\bar{\rho}}, u_\psi$ — polar components of steady-state displacements in vertical plane $y = 0$

V — velocity of moving load

x,y,z — Cartesian coordinates along X-, Y-, and Z-axes, respectively

$\bar{x} = x - Vt$

$\alpha_1^2 = \frac{3 + \sqrt{3}}{4}$

$\alpha_2^2 = \frac{3 - \sqrt{3}}{4}$

$\beta_l = \sqrt{M_l{}^2 - 1}$

$\beta_R = \sqrt{M_R{}^2 - 1}$

$\beta_t = \sqrt{M_t{}^2 - 1}$

$\gamma_1, \gamma_2, \gamma_3$ constants

$\delta(x)$ Dirac delta function

$\Delta(\lambda,\mu) = \left[2\left(\lambda^2 + \mu^2\right) - M_t{}^2\lambda^2 - 2i\epsilon V\lambda\right]^2 - 4S_l S_t\left(\lambda^2 + \mu^2 - i\epsilon V\lambda\right) = \bar{\Delta}(\lambda,\mu,V\lambda)$

$\bar{\Delta}(\lambda,\mu,\omega)$ quantity defined in equation (21)

ϵ a small positive constant

$\eta = \dfrac{2M_t{}^2\sin^2\varphi}{3 - M_t{}^2\sin^2\varphi}$

$\theta_l = \sin^{-1}\left(\dfrac{1}{M_l}\right)$

$\theta_R = \sin^{-1}\left(\dfrac{1}{M_R}\right)$

$\theta_t = \sin^{-1}\left(\dfrac{1}{M_t}\right)$

$\kappa = \dfrac{1}{k}$

λ,μ,ω transform variables

λ',μ' Lamé constants

λ_1,λ_2 Rayleigh poles

λ_1',λ_2' branch points

$\Pi(\alpha,k)$ complete elliptic integral of the third kind,

$$\int_0^{\pi/2} \frac{1}{(1 - \alpha \sin^2\theta)\sqrt{1 - k^2\sin^2\theta}}\, d\theta$$

ρ_o density of medium composing the half space

$\bar{\rho},\psi$ polar coordinates

$\sigma_{xx},\sigma_{yy},\sigma_{zz}$ normal stresses

$$\tau = \frac{c_t t}{r}$$

$\tau_{xy},\tau_{xz},\tau_{yz}$ shear stresses

$\bar{\varphi},\bar{\chi}$ stress functions

$$\Omega_l = \sqrt{\lambda^2 + \mu^2 - \frac{\omega^2}{c_l^2} - i\epsilon\omega}$$

$$\Omega_t = \sqrt{\lambda^2 + \mu^2 - \frac{\omega^2}{c_t^2} - i\epsilon\omega}$$

$\fint$ denotes an integral taken in sense of a Cauchy principal value

$\nabla^2 = \frac{\partial^2}{\partial x^2} + \frac{\partial^2}{\partial y^2} + \frac{\partial^2}{\partial z^2}$ three-dimensional Laplacian operator

STATEMENT OF THE PROBLEM

Let a concentrated load of magnitude P be applied normal to the surface of a semi-infinite elastic half-space and be moved along a straight line at a constant velocity V as shown in figure 1. Introduce a right-handed system of rectangular Cartesian coordinate axes X, Y, and Z fixed in the medium with the positive X-axis coincident with the line of motion and oriented in the direction of motion, and with the positive Z-axis pointing into the half space. The sign of the load P will be taken as positive when it acts in the direction of the positive Z-axis, that is, when the load places the adjacent surface in compression. Let u, v, and w be the displacements of any point of the medium parallel to the X-, Y-, and Z-axes, respectively. The problem to be solved in this paper is the determination of the displacements for any value of the load velocity V.

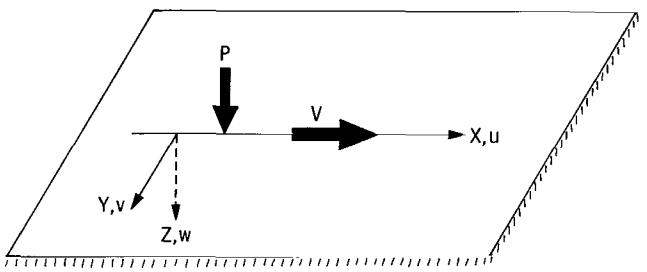

Figure 1.- Coordinate system and components of displacement.

Two aspects of this problem are considered. First, it is assumed that the load has been moving for a considerable length of time so that all transient disturbances produced at the initial point of application have died out and have left only a steady pattern of displacements with respect to an observer moving with the load. By using Fourier transform techniques or, equivalently, superpositions of plane waves, expressions are obtained from which the displacements at any depth may be calculated. Second, the complete time-dependent solution for the horizontal displacements produced at the surface of the medium is discussed. In this case, the displacements are obtained by a suitable integration in time of the response of the surface to an impulse and include the transients excited by the initial application of the load.

STEADY-STATE DISPLACEMENTS

The determination of the steady-state displacements requires finding a solution of the equations of motion (ref. 6, ch. 5)

$$\mu'\nabla^2\vec{u} + (\lambda' + \mu')\nabla(\nabla \cdot \vec{u}) = \rho_o \frac{\partial^2 \vec{u}}{\partial t^2} \tag{1}$$

which satisfies at the surface $z = 0$ the conditions that the normal stress must equal $-P\delta(y)\ \delta(x - Vt)$ and the shear stresses must vanish. In these equations $\vec{u}$ is the displacement vector $u\vec{i} + v\vec{j} + w\vec{k}$, ρ_o is the mass density of the medium (assumed to be

constant), λ' and μ' are the Lamé constants of the medium, and $\delta(y)$ and $\delta(x - Vt)$ are Dirac delta functions. A solution to this problem is obtained by expressing the displacements and stresses in terms of two stress functions and then representing the stress functions as appropriate superpositions of plane waves to satisfy the surface conditions.

Stress Functions and the Radiation Condition

As shown by Lamb (ref. 7), the equations of motion (eq. (1)) are satisfied by letting

$$\left.\begin{aligned} u &= \frac{\partial \bar{\varphi}}{\partial x} + \frac{\partial^2 \bar{\chi}}{\partial x\, \partial z} \\ v &= \frac{\partial \bar{\varphi}}{\partial y} + \frac{\partial^2 \bar{\chi}}{\partial y\, \partial z} \\ w &= \frac{\partial \bar{\varphi}}{\partial z} + \frac{\partial^2 \bar{\chi}}{\partial z^2} - \frac{1}{c_t^2} \frac{\partial^2 \bar{\chi}}{\partial t^2} \end{aligned}\right\} \tag{2}$$

provided that the two stress functions $\bar{\varphi}$ and $\bar{\chi}$ are solutions of the three-dimensional wave equations

$$\nabla^2 \bar{\varphi} = \frac{1}{c_l^2} \frac{\partial^2 \bar{\varphi}}{dt^2} \tag{3}$$

and

$$\nabla^2 \bar{\chi} = \frac{1}{c_t^2} \frac{\partial^2 \bar{\chi}}{\partial t^2} \tag{4}$$

in which $c_l^2 = \frac{1}{\rho_o}(\lambda + 2\mu')$ and $c_t^2 = \frac{1}{\rho_o}\mu'$. In terms of these stress functions the normal stresses become

$$\sigma_{xx} = \frac{\lambda'}{c_l^2} \frac{\partial^2 \bar{\varphi}}{\partial t^2} + 2\mu' \left(\frac{\partial^2 \bar{\varphi}}{\partial x^2} + \frac{\partial^3 \bar{\chi}}{\partial z\, \partial x^2} \right)$$

$$\sigma_{yy} = \frac{\lambda'}{c_l^2} \frac{\partial^2 \bar{\varphi}}{\partial t^2} + 2\mu' \left(\frac{\partial^2 \bar{\varphi}}{\partial y^2} + \frac{\partial^3 \bar{\chi}}{\partial z\, \partial y^2} \right)$$

$$\sigma_{zz} = \frac{\lambda'}{c_l^2}\frac{\partial^2\overline{\varphi}}{\partial t^2} + 2\mu'\left(\frac{\partial^2\overline{\varphi}}{\partial z^2} + \frac{\partial^3\overline{\chi}}{\partial z^3}\right) - 2\rho_o\frac{\partial^3\overline{\chi}}{\partial z\,\partial t^2} \tag{5}$$

and the shear stresses become

$$\tau_{xy} = \tau_{yx} = 2\mu'\left(\frac{\partial^2\overline{\varphi}}{\partial x\,\partial y} + \frac{\partial^3\overline{\chi}}{\partial x\,\partial y\,\partial z}\right)$$

$$\tau_{xz} = \tau_{zx} = 2\mu'\left(\frac{\partial^2\overline{\varphi}}{\partial x\,\partial z} + \frac{\partial^3\overline{\chi}}{\partial x\,\partial z^2}\right) - \rho_o\frac{\partial^3\overline{\chi}}{\partial x\,\partial t^2} \tag{6}$$

$$\tau_{yz} = \tau_{zy} = 2\mu'\left(\frac{\partial^2\overline{\varphi}}{\partial y\,\partial z} + \frac{\partial^3\overline{\chi}}{\partial y\,\partial z^2}\right) - \rho_o\frac{\partial^3\overline{\chi}}{\partial y\,\partial t^2} \tag{7}$$

where c_l is the speed of propagation of longitudinal compression waves which are referred to as P-waves and c_t is the speed of propagation of transverse shear waves referred to as S-waves. (See ref. 6, ch. 13.) Both of these waves are three-dimensional body waves which spread through the interior of the medium and decay as the reciprocal of the distance from the source.

In addition to these two types of waves, the presence of a free surface on the solid gives rise to a third type of wave known as a Rayleigh wave or R-wave. (See ref. 6, ch. 13.) This wave is a surface wave similar to a gravity wave on water. It involves both compression and shear. The Rayleigh wave is essentially two dimensional; its strength falls off rapidly with depth and the energy it carries is confined to a thin layer near the surface.

As will be seen subsequently, the three wave speeds c_R, c_t, and c_l play an important role in determining the nature of the displacement pattern. The P-wave is the fastest traveling wave. The Rayleigh wave travels with a speed c_R which is slightly less than the shear wave speed.

Besides satisfying the imposed boundary conditions, the solution of the present problem must also satisfy the radiation condition which is the physical requirement that only outgoing waves are observed at a great distance from the applied load. (See ref. 8.) As discussed in reference 9 this condition may be taken into account by adding the terms $\epsilon\frac{\partial\overline{\varphi}}{\partial t}$ and $\epsilon\frac{\partial\overline{\chi}}{\partial t}$ (with ϵ positive) to the right-hand side of equations (3) and (4), respectively, and considering the original problem as the limiting case ϵ approaching 0.

Accordingly, in place of equations (3) and (4), it is advantageous to deal with the equations

$$\nabla^2 \bar{\varphi} = \frac{1}{c_l^2} \frac{\partial^2 \bar{\varphi}}{\partial t^2} + \epsilon \frac{\partial \bar{\varphi}}{\partial t} \tag{8}$$

and

$$\nabla^2 \bar{\chi} = \frac{1}{c_t^2} \frac{\partial^2 \bar{\chi}}{\partial t^2} + \epsilon \frac{\partial \bar{\chi}}{\partial t} \tag{9}$$

These equations possess plane-wave solutions of the form

$$\bar{\varphi} = e^{i\lambda x + i\mu y - z\Omega_l - i\omega t}$$

and

$$\bar{\chi} = e^{i\lambda x + i\mu y - z\Omega_t - i\omega t}$$

where

$$\Omega_l = \sqrt{\lambda^2 + \mu^2 - \frac{\omega^2}{c_l^2} - i\omega\epsilon}$$

and

$$\Omega_t = \sqrt{\lambda^2 + \mu^2 - \frac{\omega^2}{c_t^2} - i\omega\epsilon}$$

Since equations (8) and (9) are linear, these simple solutions may be superimposed by summation or integration to construct more general solutions.

For present purposes it is convenient to assume the following forms for the stress functions:

$$\bar{\varphi} = \int_{-\infty}^{+\infty} \int_{-\infty}^{+\infty} \int_{-\infty}^{+\infty} f(\lambda,\mu,\omega) e^{i\lambda x + i\mu y - i\omega t - z\Omega_l} \, d\lambda \, d\mu \, d\omega \tag{10}$$

$$\bar{\chi} = \int_{-\infty}^{+\infty} \int_{-\infty}^{+\infty} \int_{-\infty}^{+\infty} g(\lambda,\mu,\omega) e^{i\lambda x + i\mu y - i\omega t - z\Omega_t} \, d\lambda \, d\mu \, d\omega \tag{11}$$

In equations (10) and (11), $f(\lambda,\mu,\omega)$ and $g(\lambda,\mu,\omega)$ are arbitrary functions. Once these functions have been determined so that the boundary conditions at the surface are satisfied, the displacements may be found from equation (2). The necessary steps in finding f and g and then u, v, and w are now carried out.

Formal Solution for Displacements

The boundary conditions to be satisfied at $z = 0$ are

$$\sigma_{zz} = -P\delta(y)\delta(x - Vt) \tag{12}$$

and

$$\tau_{xz} = \tau_{yz} = 0 \tag{13}$$

From equations (6) and (7) it is seen that equation (13) can be satisfied by setting

$$2\left(\frac{\partial \overline{\varphi}}{\partial z} + \frac{\partial^2 \overline{\chi}}{\partial z^2}\right) - \frac{1}{c_t^2}\frac{\partial^2 \overline{\chi}}{\partial t^2} = 0 \tag{14}$$

at $z = 0$. Equations (14), (5), and (12) give two conditions for determining the unknown functions f and g. If the expressions for $\overline{\varphi}$ and $\overline{\chi}$ (eqs. (10) and (11) are substituted into equations (5) and (14) and z is set equal to zero, one obtains, with the aid of equation (12),

$$-P\delta(y)\delta(x - Vt) = \int_{-\infty}^{+\infty}\int_{-\infty}^{+\infty}\int_{-\infty}^{+\infty}\left[f\left(2\mu'\Omega_l^2 - \frac{\omega^2\lambda'}{c_l^2}\right) - 2\Omega_t\mu' g\left(\Omega_t^2 + \frac{\omega^2}{c_t^2}\right)\right]e^{i\lambda x + i\mu y - i\omega t}\, d\lambda\, d\mu\, d\omega \tag{15}$$

and

$$0 = \int_{-\infty}^{+\infty}\int_{-\infty}^{+\infty}\int_{-\infty}^{+\infty}\left[2\Omega_l f - g\left(2\Omega_t^2 + \frac{\omega^2}{c_t^2}\right)\right]e^{i\lambda x + i\mu y - i\omega t}\, d\lambda\, d\mu\, d\omega \tag{16}$$

Equations (16) and (15) may be solved for the terms in brackets in the integrands by means of the Fourier inversion formulas (ref. 10):

$$2\Omega_l f - g\left(2\Omega_t^2 + \frac{\omega^2}{c_t^2}\right) = 0 \tag{17}$$

and

$$f\left(2\mu'\Omega_l^2 - \lambda'\frac{\omega^2}{c_l^2}\right) - 2\Omega_t\mu'\left(\Omega_t^2 + \frac{\omega^2}{c_t^2}\right)g$$

$$= -\frac{P}{(2\pi)^3}\int_{-\infty}^{+\infty}\int_{-\infty}^{+\infty}\int_{-\infty}^{+\infty}\delta(y)\,\delta(x - Vt)e^{-i\lambda x - i\mu y + i\omega t}\,dx\,dy\,dt$$

$$= -\frac{P}{(2\pi)^2}\,\delta(\omega - V\lambda) \tag{18}$$

When solved for f and g, equations (17) and (18) give

$$f = \frac{-P'}{(2\pi)^2}\,\frac{2\Omega_t^2 + \frac{\omega^2}{c_t^2}}{\bar{\Delta}(\lambda,\mu,\omega)}\,\delta(\omega - V\lambda) \tag{19}$$

$$g = \frac{-P'}{(2\pi)^2}\,\frac{2\Omega_l}{\bar{\Delta}(\lambda,\mu,\omega)}\,\delta(\omega - V\lambda) \tag{20}$$

where $P' = \frac{P}{\mu'}$ and

$$\bar{\Delta}(\lambda,\mu,\omega) = \left[2(\lambda^2 + \mu^2) - \frac{\omega^2}{c_t^2} - 2i\epsilon\omega\right]^2 - 4\Omega_l\,\Omega_t(\lambda^2 + \mu^2 - i\epsilon\omega) \tag{21}$$

The stress functions $\bar{\varphi}$ and $\bar{\chi}$ are now determined by substituting equations (19) and (20) into equations (10) and (11). The integration with respect to ω is easily performed and yields

$$\bar{\varphi} = \frac{-P'}{4\pi^2}\int_{-\infty}^{+\infty}\int_{-\infty}^{+\infty}\frac{2S_t^2 + M_t^2\lambda^2}{\Delta(\lambda,\mu)}\,e^{i\lambda\bar{x} + i\mu y - zS_l}\,d\lambda\,d\mu \tag{22}$$

and

$$\bar{\chi} = \frac{-P'}{4\pi^2}\int_{-\infty}^{+\infty}\int_{-\infty}^{+\infty}\frac{2S_l}{\Delta(\lambda,\mu)}\,e^{i\lambda\bar{x} + i\mu y - zS_t}\,d\lambda\,d\mu \tag{23}$$

where

$$\bar{x} = x - Vt$$

$$M_l = \frac{V}{c_l}$$

$$M_t = \frac{V}{c_t}$$

$$S_l^2 = \lambda^2 + \mu^2 - M_l^2\lambda^2 - iV\epsilon\lambda$$

$$S_t^2 = \lambda^2 + \mu^2 - M_t^2\lambda^2 - iV\epsilon\lambda$$

and, from equation (21),

$$\Delta(\lambda,\mu) = \bar{\Delta}(\lambda,\mu,\lambda V) = \left[2(\lambda^2 + \mu^2) - M_t^2\lambda^2 - 2i\epsilon V\lambda\right]^2 - 4S_l S_t(\lambda^2 + \mu^2 - i\epsilon V\lambda)$$

The displacements obtained by substituting equations (22) and (23) into equation (2) are

$$u(\bar{x},y,z) = \frac{-P'i}{4\pi^2}\int_{-\infty}^{+\infty}\int_{-\infty}^{+\infty}\frac{\lambda e^{i\lambda\bar{x}+i\mu y}}{\Delta(\lambda,\mu)}\left[(2S_t^2 + M_t^2\lambda^2)e^{-zS_l} - 2S_l S_t e^{-zS_t}\right]d\lambda\, d\mu \qquad (24)$$

$$v(\bar{x},y,z) = \frac{-P'i}{4\pi^2}\int_{-\infty}^{+\infty}\int_{-\infty}^{+\infty}\frac{\mu e^{i\lambda\bar{x}+i\mu y}}{\Delta(\lambda,\mu)}\left[(2S_t^2 + M_t^2\lambda^2)e^{-zS_l} - 2S_l S_t e^{-zS_t}\right]d\lambda\, d\mu \qquad (25)$$

$$w(\bar{x},y,z) = \frac{P'}{4\pi^2}\int_{-\infty}^{+\infty}\int_{-\infty}^{+\infty}\frac{S_l e^{i\lambda\bar{x}+i\mu y}}{\Delta(\lambda,\mu)}\left[(2S_t^2 + M_t^2\lambda^2)e^{-zS_l} - 2(S_t^2 + M_t^2\lambda^2)e^{-zS_t}\right]d\lambda\, d\mu \qquad (26)$$

Since these expressions depend upon t only through the variable $\bar{x}$, the displacement pattern is steady in time for an observer moving with the load.

Equations (24) to (26) are the general expressions for the displacements valid for any depth, load speed, or elastic constants. In particular, when $V = 0$, these equations reproduce the classical solution of the problem of Boussinesq. (See ref. 6, ch. 8.) In addition, it is now a straightforward matter to obtain corresponding integrals for the stresses and strains produced within the medium. This phase of the problem will not be pursued here and attention will be focused on the displacements only.

The integrands of equations (24) to (26) are, in general, multiple-valued functions because of the presence of the radicals S_l and S_t and become infinite at the so-called Rayleigh poles which occur at a certain pair of simple zeros of $\Delta(\lambda,\mu)$. Therefore, the value of the radicals must be defined and the manner of integrating around the poles must be determined before the integrals can be evaluated numerically or simplified by carrying

out some of the integrations in closed form. The proper treatment of these singularities which is necessary to obtain a physically acceptable result requires a detailed study of the poles and branch points of the integrands and depends upon the values of the elastic constants λ' and μ' (or equivalently, c_l and c_t) and load velocity. It is in this investigation that the positive parameter ϵ plays a significant role.

In general, it is found that the expressions for the displacements can be written in the form

$$(u,v,w) = (u',v',w') + (u'',v'',w'') \tag{27}$$

The terms u', v', and w' are associated with the Rayleigh poles and must be taken into account whenever the load speed exceeds the Rayleigh wave speed. To obtain explicit expressions for these quantities, one must determine the zeros of $\Delta(\lambda,\mu)$. This determination of zeros requires some assumption for the value of the ratio of elastic constants λ' and μ' or for the value of the ratio of the wave speeds c_l and c_t. The terms u'', v'', and w'' are integrals of the same form as those in equations (24), (25), and (26) but are taken in the sense of Cauchy principal values. These double integrals with infinite limits can be expressed in terms of single integrals with finite limits by transforming from the "rectangular" coordinate system λ,μ to a "polar" coordinate system r,θ and then carrying out the r-integration. The results do not depend upon any assumptions for the values of the elastic constants or wave speeds. The integrands and limits of the remaining θ integrals take various forms depending on whether $V < c_t$, the subseismic case; $c_t < V < c_l$, transeismic case; or $c_l < V$, the superseismic case. Explicit expressions for the quantities u'', v'', and w'' in the three different cases are given in the next section.

Single Finite Integrals for u'', v'', and w''

In this section single integrals with finite limits are presented for the quantities u'', v'', and w''. The detailed steps leading from equations (24), (25), and (26) to these results are given in the appendix. In the following equations $\theta_t = \sin^{-1}\frac{1}{M_t}$ and $\theta_l = \sin^{-1}\frac{1}{M_l}$. The symbol $\oint d\theta$ indicates that an integral is to be understood in the sense of a Cauchy principal value. The parameter ϵ does not appear in the final equations; its only purpose is to determine the manner of handling the branch points and poles. Once this is done, as in the appendix, ϵ is set equal to zero.

The desired expressions for single integrals with finite limits are:

Subseismic case; $0 < V < c_t$, $M_l < M_t < 1$:

$$u''(\bar{x},y,z) = \frac{P'}{\pi^2} \oint_0^{\pi/2} u_1(\bar{x},y,z;\theta)d\theta \tag{28}$$

$$v''(\bar{x},y,z) = \frac{P'}{\pi^2} \oint_0^{\pi/2} v_1(\bar{x},y,z;\theta)d\theta \tag{29}$$

$$w''(\bar{x},y,z) = \frac{P'}{\pi^2} \oint_0^{\pi/2} w_1(\bar{x},y,z;\theta)d\theta \tag{30}$$

Transeismic case; $c_t < V < c_l$, $M_l < 1 < M_t$:

$$u''(\bar{x},y,z) = \frac{P'}{\pi^2}\left[\oint_0^{\theta_t} u_1(\bar{x},y,z;\theta)d\theta + \oint_{\theta_t}^{\pi/2} u_2(\bar{x},y,z;\theta)d\theta\right] \tag{31}$$

$$v''(\bar{x},y,z) = \frac{P'}{\pi^2}\left[\oint_0^{\theta_t} v_1(\bar{x},y,z;\theta)d\theta + \oint_{\theta_t}^{\pi/2} v_2(\bar{x},y,z;\theta)d\theta\right] \tag{32}$$

$$w''(\bar{x},y,z) = \frac{P'}{\pi^2}\left[\oint_0^{\theta_t} w_1(\bar{x},y,z;\theta)d\theta + \oint_{\theta_t}^{\pi/2} w_2(\bar{x},y,z;\theta)d\theta\right] \tag{33}$$

Superseismic case; $c_t < c_l < V$, $1 < M_l < M_t$:

$$u''(\bar{x},y,z) = \frac{P'}{\pi^2}\left[\oint_0^{\theta_t} u_1(\bar{x},y,z;\theta)d\theta + \oint_{\theta_t}^{\theta_l} u_2(\bar{x},y,z;\theta)d\theta + \oint_{\theta_l}^{\pi/2} u_3(\bar{x},y,z;\theta)d\theta\right] \tag{34}$$

$$v''(\bar{x},y,z) = \frac{P'}{\pi^2}\left[\oint_0^{\theta_t} v_1(\bar{x},y,z;\theta)d\theta + \oint_{\theta_t}^{\theta_l} v_2(\bar{x},y,z;\theta)d\theta + \oint_{\theta_l}^{\pi/2} v_3(\bar{x},y,z;\theta)d\theta\right] \tag{35}$$

$$w''(\bar{x},y,z) = \frac{P'}{\pi^2}\left[\oint_0^{\theta_t} w_1(\bar{x},y,z;\theta)d\theta + \oint_{\theta_t}^{\theta_l} w_2(\bar{x},y,z;\theta)d\theta + \oint_{\theta_l}^{\pi/2} w_3(\bar{x},y,z;\theta)d\theta\right] \tag{36}$$

in which

$$u_1(\bar{x},y,z;\theta) = \frac{\sin\theta}{A^2(\theta) - 4B(\theta)}\left[\frac{A(\theta)}{2} S^+\left(z\sqrt{1 - M_l{}^2\sin^2\theta},\bar{x}\sin\theta,y\cos\theta\right)\right.$$
$$\left. - B(\theta)S^+\left(z\sqrt{1 - M_t{}^2\sin^2\theta},\bar{x}\sin\theta,y\cos\theta\right)\right] \tag{37}$$

$$v_1(\bar{x},y,z;\theta) = \frac{\cos\theta}{A^2(\theta) - 4B(\theta)}\left[\frac{A(\theta)}{2} S^+\left(z\sqrt{1 - M_l{}^2\sin^2\theta},y\cos\theta,\bar{x}\sin\theta\right)\right.$$
$$\left. - B(\theta)S^+\left(z\sqrt{1 - M_t{}^2\sin^2\theta},y\cos\theta,\bar{x}\sin\theta\right)\right] \tag{38}$$

$$w_1(\bar{x},y,z;\theta) = \frac{\sqrt{1 - M_l{}^2\sin^2\theta}}{A^2(\theta) - 4B(\theta)}\left[\frac{A(\theta)}{2} C^+\left(z\sqrt{1 - M_l{}^2\sin^2\theta},\bar{x}\sin\theta,y\cos\theta\right)\right.$$
$$\left. - C^+\left(z\sqrt{1 - M_t{}^2\sin^2\theta},\bar{x}\sin\theta,y\cos\theta\right)\right] \tag{39}$$

$$u_2(\bar{x},y,z;\theta) = \frac{\sin\theta}{A^4(\theta) + 16C^2(\theta)}\left\{\frac{A^3(\theta)}{2} S^+\left(z\sqrt{1 - M_l{}^2\sin^2\theta},\bar{x}\sin\theta,y\cos\theta\right)\right.$$
$$- 2A(\theta)C(\theta)C^+\left(z\sqrt{1 - M_l{}^2\sin^2\theta},\bar{x}\sin\theta,y\cos\theta\right)$$
$$+ \pi A^2(\theta)C(\theta)\left[\delta\left(\bar{x}\sin\theta + y\cos\theta + z\sqrt{M_t{}^2\sin^2\theta - 1}\right)\right.$$
$$\left. + \delta\left(\bar{x}\sin\theta - y\cos\theta + z\sqrt{M_t{}^2\sin^2\theta - 1}\right)\right]$$
$$\left. + 8C^2(\theta)\frac{\bar{x}\sin\theta + z\sqrt{M_t{}^2\sin^2\theta - 1}}{\left(\bar{x}\sin\theta + z\sqrt{M_t{}^2\sin^2\theta - 1}\right)^2 - y^2\cos^2\theta}\right\} \tag{40}$$

$$v_2(\bar{x},y,z;\theta) = \frac{\cos\theta}{A^4(\theta) + 16C^2(\theta)} \left\{ \frac{A^3(\theta)}{2} S^+\left(z\sqrt{1 - M_l{}^2\sin^2\theta}, y\cos\theta, \bar{x}\sin\theta\right) \right.$$

$$+ 2A(\theta)C(\theta)C^-\left(z\sqrt{1 - M_l{}^2\sin^2\theta}, y\cos\theta, \bar{x}\sin\theta\right)$$

$$- \pi A^2(\theta)C(\theta)\left[\delta\left(\bar{x}\sin\theta - y\cos\theta + z\sqrt{M_t{}^2\sin^2\theta - 1}\right)\right.$$

$$\left. - \delta\left(\bar{x}\sin\theta + y\cos\theta + z\sqrt{M_t{}^2\sin^2\theta - 1}\right)\right]$$

$$\left. - 8C^2(\theta) \frac{y\cos\theta}{\left(\bar{x}\sin\theta + z\sqrt{M_t{}^2\sin^2\theta - 1}\right)^2 - y^2\cos^2\theta} \right\} \tag{41}$$

$$w_2(\bar{x},y,z;\theta) = \frac{\sqrt{1 - M_l{}^2\sin^2\theta}}{A^4(\theta) + 16C^2(\theta)} \left\{ \frac{A^3(\theta)}{2} C^+\left(z\sqrt{1 - M_l{}^2\sin^2\theta}, \bar{x}\sin\theta, y\cos\theta\right) \right.$$

$$+ 2A(\theta)C(\theta)S^+\left(z\sqrt{1 - M_l{}^2\sin^2\theta}, \bar{x}\sin\theta, y\cos\theta\right)$$

$$- \pi A^2(\theta)\left[\delta\left(\bar{x}\sin\theta + y\cos\theta + z\sqrt{M_t{}^2\sin^2\theta - 1}\right)\right.$$

$$\left. + \delta\left(\bar{x}\sin\theta - y\cos\theta + z\sqrt{M_t{}^2\sin^2\theta - 1}\right)\right]$$

$$\left. - 8C(\theta) \frac{\bar{x}\sin\theta + z\sqrt{M_t{}^2\sin^2\theta - 1}}{\left(\bar{x}\sin\theta + z\sqrt{M_t{}^2\sin^2\theta - 1}\right)^2 - y^2\cos^2\theta} \right\} \tag{42}$$

$$u_3(\bar{x},y,z;\theta) = \frac{\sin\theta}{A^2(\theta) + 4D(\theta)} \left[A(\theta) \frac{\bar{x}\sin\theta + z\sqrt{M_l{}^2\sin^2\theta - 1}}{\left(\bar{x}\sin\theta + z\sqrt{M_l{}^2\sin^2\theta - 1}\right)^2 - y^2\cos^2\theta} + 2D(\theta) \frac{\bar{x}\sin\theta + z\sqrt{M_t{}^2\sin^2\theta - 1}}{\left(\bar{x}\sin\theta + z\sqrt{M_t{}^2\sin^2\theta - 1}\right)^2 - y^2\cos^2\theta} \right] \tag{43}$$

$$v_3(\bar{x},y,z;\theta) = \frac{-\cos\theta}{A^2(\theta) + 4D(\theta)} \left[A(\theta) \frac{y\cos\theta}{\left(\bar{x}\sin\theta + z\sqrt{M_l{}^2\sin^2\theta - 1}\right)^2 - y^2\cos^2\theta} + 2D(\theta) \frac{y\cos\theta}{\left(\bar{x}\sin\theta + z\sqrt{M_t{}^2\sin^2\theta - 1}\right)^2 - y^2\cos^2\theta} \right] \tag{44}$$

$$w_3(\bar{x},y,z;\theta) = \frac{\sqrt{M_l{}^2\sin^2\theta - 1}}{A^2(\theta) + 4D(\theta)} \left[A(\theta) \frac{\bar{x}\sin\theta + z\sqrt{M_l{}^2\sin^2\theta - 1}}{\left(\bar{x}\sin\theta + z\sqrt{M_l{}^2\sin^2\theta - 1}\right)^2 - y^2\cos^2\theta} - 2 \frac{\bar{x}\sin\theta + z\sqrt{M_t{}^2\sin^2\theta - 1}}{\left(\bar{x}\sin\theta + z\sqrt{M_t{}^2\sin^2\theta - 1}\right)^2 - y^2\cos^2\theta} \right] \tag{45}$$

$$\left.\begin{aligned} A(\theta) &= 2 - M_t^2 \sin^2\theta \\ B(\theta) &= \sqrt{1 - M_t^2 \sin^2\theta}\sqrt{1 - M_l^2 \sin^2\theta} \\ C(\theta) &= \sqrt{M_t^2 \sin^2\theta - 1}\sqrt{1 - M_l^2 \sin^2\theta} \\ D(\theta) &= \sqrt{M_t^2 \sin^2\theta - 1}\sqrt{M_l^2 \sin^2\theta - 1} \end{aligned}\right\} \tag{46}$$

and

$$\left.\begin{aligned} S^+(a,b,c) &= \frac{b - c}{a^2 + (b - c)^2} + \frac{b + c}{a^2 + (b + c)^2} \\ C^+(a,b,c) &= \frac{a}{a^2 + (b - c)^2} + \frac{a}{a^2 + (b + c)^2} \\ C^-(a,b,c) &= \frac{a}{a^2 + (b - c)^2} - \frac{a}{a^2 + (b + c)^2} \end{aligned}\right\} \tag{47}$$

When $c_R < V$, the integrals of u_1, v_1, and w_1 are singular since $A^2(\theta) - 4B(\theta)$ vanishes when $\theta = \theta_R = \sin^{-1}\frac{c_R}{V}$ which is smaller than either of the upper limits θ_t or $\pi/2$. The integrals of the delta functions in u_2, v_2, and w_2 can be carried out analytically by means of the following formula (ref. 11):

$$\int_a^b f(\theta)\delta(g(\theta))d\theta = \sum_i \frac{f(\theta_i)}{|g'(\theta_i)|} \tag{48}$$

in which the summation extends over all the zeros of $g(\theta)$, the θ_i values, which lie between the upper and lower limits of integration, a and b. Equations equivalent to equations (28) to (30) and (37) to (39) for the subseismic case are given in reference 4. However, the terms which must be added to these integrals to obtain the displacements when $c_R < V < c_t$ are not indicated.

Expressions for u', v', and w' When Poisson's Ratio Is 1/4

In the remainder of this paper it is assumed that Poisson's ratio is 1/4; thus, $\lambda' = \mu' = 2/5$ Young's modulus. The relation between the P-wave speed c_l and the S-wave speed c_t is then $c_l = \sqrt{3}c_t$; thus, the compression waves travel with a speed about 70 percent greater than that of the shear waves. The relation between the Rayleigh wave speed c_R and the S-wave speed is $c_R = \frac{2}{\sqrt{3 + \sqrt{3}}} c_t \approx 0.92c_t$.

This assumption is reasonably close to the truth for many materials. Moreover, the steps involved in obtaining explicit expressions for u', v', and w' in this special case indicate the procedure to be followed when other values of λ' and μ' are of interest. The details are worked out in the appendix; only the final results are given here. When the equations are presented, it is convenient to use the abbreviations:

$$M_R = \frac{V}{c_R}$$

$$\beta_R = \sqrt{M_R^2 - 1}$$

$$\alpha_1^2 = \frac{3 + \sqrt{3}}{4}$$

$$\alpha_2^2 = \frac{3 - \sqrt{3}}{4}$$

Again it should be noticed that the parameter ϵ does not appear in the final results.

The additional terms arising from the Rayleigh poles when Poisson's ratio is 1/4 are:

$$\left.\begin{aligned}
u'(\bar{x},y,z) &= \frac{-P'\alpha_1^2}{8\pi\beta_R}\left[C^+\left(zM_t\sqrt{\alpha_1^2 - 1/3},\bar{x},\beta_R y\right) - \frac{1}{\sqrt{3}} C^+\left(zM_t\sqrt{\alpha_1^2 - 1},\bar{x},\beta_R y\right)\right] \\
v'(\bar{x},y,z) &= \frac{P'\alpha_1^2}{8\pi}\left[C^-\left(zM_t\sqrt{\alpha_1^2 - 1/3},\bar{x},\beta_R y\right) - \frac{1}{\sqrt{3}} C^-\left(zM_t\sqrt{\alpha_1^2 - 1},\bar{x},\beta_R y\right)\right] \\
w'(\bar{x},y,z) &= \frac{P'M_t\alpha_1^2\sqrt{\alpha_1^2 - 1/3}}{8\pi\beta_R}\left[S^+\left(zM_t\sqrt{\alpha_1^2 - 1/3},\bar{x},\beta_R y\right) - \sqrt{3}S^+\left(zM_t\sqrt{\alpha_1^2 - 1},\bar{x},\beta_R y\right)\right]
\end{aligned}\right\} \tag{49}$$

in which $C^+(a,b,c)$, $C^-(a,b,c)$, and $S^+(a,b,c)$ are the combinations of elementary functions defined in equation (47). These terms must be included in equation (27) for the displacements when $M_R > 1$ and are to be ignored when $M_R < 1$. In particular, at the surface ($z = 0$)

$$u'(\bar{x},y,0) = v'(\bar{x},y,0) = 0$$

and

$$w'(\bar{x},y,0) = -\frac{P'M_t\sqrt{5 + 3\sqrt{3}}}{16\pi\beta_R} \frac{\bar{x}}{\bar{x}^2 - \beta_R{}^2 y^2} \tag{50}$$

Equation (49) and the expressions for the stresses associated with these "displacements" can be used without the additional and more complicated terms u'', v'', and w'' to estimate the main effects near the surface at large distances from the moving load when $V > c_R$. (Similar terms could be obtained when $V < c_R$ but these terms are not needed in the present investigation.) The rationale for this approximate and simplified procedure is discussed in reference 12 for a time-dependent half-space problem and will not be discussed further. The results obtained in that paper are applied to a nuclear blast problem in reference 13.

Equations for the Surface Displacements

In order to obtain some indication of the magnitude and significant features of the displacement pattern in the three possible speed ranges, z was set equal to zero in the integrals for u'', v'', and w'' and the results added to equation (50) to give the displacements at the surface of the elastic half-space. The equations for this special case are presented in this section. Some numerical results based on these equations are discussed subsequently.

The process of simplifying the integrals for u'', v'', and w'' when $z = 0$ is straightforward. The main steps involved in evaluating the types of integrals encountered can be summarized as follows:

(a) Integrals of rational functions of $\sin\theta$, $\cos\theta$, $\sqrt{M_t{}^2\sin^2\theta - 1}$, $\sqrt{M_l{}^2\sin^2\theta - 1}$, $\sqrt{1 - M_t{}^2\sin^2\theta}$, and $\sqrt{1 - M_l{}^2\sin^2\theta}$ can be expressed in terms of elliptic integrals and elementary functions by decomposing the integrand into partial fractions and then making use of the formulas and transformations given in reference 14.

(b)

$$\lim_{z \to 0^+} \int_a^b f(\theta) \frac{z}{z^2 + g^2(\theta)} d\theta = \pi \int_a^b f(\theta)\, \delta(g(\theta)) d\theta$$

(See ref. 11.)

(c)

$$\int_a^b f(\theta)\, \delta(g(\theta)) d\theta$$

can be expressed in terms of elementary functions by using equation (48).

When the equations for the surface displacements are written, some simplification is attained by giving the radial and tangential components of the horizontal displacements $u_{\bar{r}}$ and u_φ rather than the longitudinal and transverse components u and v. The radial and tangential components are defined as follows: Introduce a system of plane polar coordinates $\bar{r},\varphi$ on the surface of the half-space related to the Cartesian coordinates by the equations $\bar{x} = \bar{r} \cos \varphi$ and $y = \bar{r} \sin \varphi$ as shown in figure 2. The origin is thus always located at the instantaneous position of the moving load. The angle φ is measured positive clockwise as seen from above the surface, $\varphi = 0$ in the direction of motion, and $\bar{r}$ is the distance from the moving load. Then

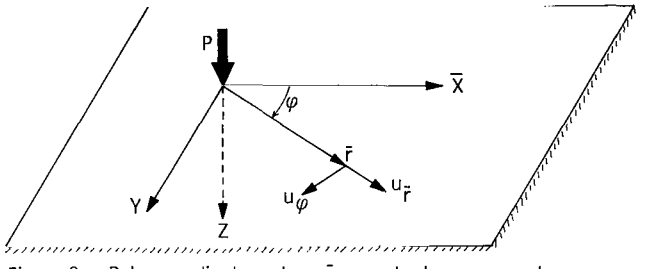

Figure 2.- Polar coordinate system $\bar{r},\varphi$ and polar components $u_{\bar{r}},u_\varphi$ of horizontal surface displacements. $\bar{r} = \sqrt{\bar{x}^2 + y^2}$; $\tan \varphi = y/\bar{x}$.

$$u_{\bar{r}} = u(\bar{x},y,0)\cos \varphi + v(\bar{x},y,0)\sin \varphi$$

$$u_\varphi = v(\bar{x},y,0)\cos \varphi - u(\bar{x},y,0)\sin \varphi$$

The radial component $u_{\bar{r}}$ is positive when the displacement is outward along a line through the position of the load. The tangential component u_φ is positive when the displacement is clockwise as seen from above the surface.

The horizontal and vertical components of the surface displacements are:

Subseismic case; $0 < V < c_t$, $M_l < M_t < 1$:

$$u_{\bar{r}} = \frac{P'}{\bar{r}}\left\{\frac{1}{16\pi^2\sqrt{1 - M_l^2}}\left[-6K(k) + 18\Pi\left(\gamma_1,k\right) - \left(6 - 4\sqrt{3}\right)\Pi\left(\gamma_2,k\right) - \left(6 + 4\sqrt{3}\right)\Pi\left(\gamma_3,k\right)\right]\right.$$

$$\left. - \frac{1}{8\pi\sqrt{1 - M_R^2}}\right\} \tag{51}$$

$$u_{\varphi} = \frac{P'}{\bar{r}}\left\{\frac{\sin\varphi\cos\varphi}{16\pi^2\sqrt{1 - M_l^2}}\left[-\frac{\frac{9}{2}M_t^2}{1 - \frac{1}{4}M_t^2\sin^2\varphi}\Pi\left(\gamma_1,k\right) + \frac{\left(6 - 4\sqrt{3}\right)\alpha_1^2M_t^2}{1 - \alpha_1^2M_t^2\sin^2\varphi}\Pi\left(\gamma_2,k\right)\right.\right.$$

$$\left.\left. + \frac{\left(6 - 4\sqrt{3}\right)\alpha_2^2M_t^2}{1 - \alpha_2^2M_t^2\sin^2\varphi}\Pi\left(\gamma_3,k\right) - \frac{6}{\sin^2\varphi}K(k) + 3\frac{\left(1 - M_t^2\sin^2\varphi\right)\left(2 - M_t^2\sin^2\varphi\right)}{\sin^2\varphi T(\varphi)}\Pi(\eta,k)\right]\right.$$

$$\left. + \frac{\sin\varphi\cos\varphi}{8\pi\sqrt{1 - M_R^2}}\frac{\alpha_1^2M_t^2}{\left(1 - \alpha_1^2M_t^2\sin^2\varphi\right)}\right\} \tag{52}$$

$$w = \frac{P'}{\bar{r}}\left\{\frac{3}{64\pi T(\varphi)}\left[\left(2 - M_t^2\sin^2\varphi\right)^2\sqrt{1 - M_l^2\sin^2\varphi} + 4\left(1 - M_l^2\sin^2\varphi\right)\sqrt{1 - M_t^2\sin^2\varphi}\right]\right.$$

$$\left. - \frac{M_t\sqrt{5 + 3\sqrt{3}}}{16\pi\sqrt{M_R^2 - 1}}\frac{\cos\varphi}{1 - \alpha_1^2M_t^2\cos^2\varphi}\right\} \tag{53}$$

Transeismic case; $c_t < V < c_l$, $M_l < 1 < M_t$:

$$u_{\bar{r}} = \frac{P'}{\bar{r}}\frac{\sqrt{\frac{3}{2}}}{16\pi^2M_t}\left[-6K(\kappa) + 18\Pi\left(\gamma_1\kappa^2,\kappa\right) - \left(6 - 4\sqrt{3}\right)\Pi\left(\gamma_2\kappa^2,\kappa\right) - \left(6 + 4\sqrt{3}\right)\Pi\left(\gamma_3\kappa^2,\kappa\right)\right] \tag{54}$$

$$u_\varphi = \frac{P'}{\bar{r}}\left\{\frac{\sqrt{\frac{3}{2}}\sin\varphi\cos\varphi}{16\pi^2 M_t}\left[\frac{-\frac{9}{2}M_t^2}{1-\frac{1}{4}M_t^2\sin^2\varphi}\Pi\left(\gamma_1\kappa^2,\kappa\right)+\frac{\left(6-4\sqrt{3}\right)\alpha_1^2M_t^2}{1-\alpha_1^2M_t^2\sin^2\varphi}\Pi\left(\gamma_2\kappa^2,\kappa\right)\right.\right.$$

$$\left.\left.+\frac{\left(6+4\sqrt{3}\right)\alpha_2^2M_t^2}{1-\alpha_2^2M_t^2\sin^2\varphi}\Pi\left(\gamma_3\kappa^2,\kappa\right)-\frac{6K(\kappa)}{\sin^2\varphi}+3\frac{\left(1-M_t^2\sin^2\varphi\right)\left(2-M_t^2\sin^2\varphi\right)}{\sin^2\varphi T(\varphi)}\Pi\left(\eta\kappa^2,\kappa\right)\right]\right.$$

$$\left.-\frac{3}{16\pi}H(-\cos\varphi)\operatorname{sgn}(\sin\varphi)\frac{\left(2-M_t^2\sin^2\varphi\right)\sqrt{1-M_l^2\sin^2\varphi}\sqrt{M_t^2\sin^2\varphi-1}}{T(\varphi)}\right\} \tag{55}$$

$$w = \frac{P'}{32\pi\bar{r}}\left\{\frac{3}{2T(\varphi)}\left[\left(2-M_t^2\sin^2\varphi\right)^2\sqrt{1-M_l^2\sin^2\varphi}+8\left(1-M_l^2\sin^2\varphi\right)\sqrt{1-M_t^2\sin^2\varphi}H(-\cos\varphi)\right]\right.$$

$$-M_t\cos\varphi\left[\frac{\sqrt{3}}{\sqrt{1-\frac{1}{4}M_t^2}}\frac{1}{1-\frac{1}{4}M_t^2\sin^2\varphi}+\frac{\sqrt{5+3\sqrt{3}}}{\sqrt{\alpha_1^2M_t^2-1}}\frac{1}{1-\alpha_1^2M_t^2\sin^2\varphi}\right.$$

$$\left.\left.-\frac{\sqrt{3\sqrt{3}-5}}{\sqrt{1-\alpha_2^2M_t^2}}\frac{1}{1-\alpha_2^2M_t^2\sin^2\varphi}\right]\right\} \tag{56}$$

Superseismic case; $c_t < c_l < V$, $1 < M_l < M_t$:

$$u_{\bar{r}} = 0$$

$$u_\varphi = -\frac{3P'}{16\pi\bar{r}}H(-\cos\varphi)\operatorname{sgn}(\sin\varphi)\frac{\sqrt{1-M_l^2\sin^2\varphi}\sqrt{M_t^2\sin^2\varphi-1}\left(2-M_t^2\sin^2\varphi\right)}{T(\varphi)} \tag{57}$$

$$w = \frac{3P'}{32\pi\bar{r}}H(-\cos\varphi)\frac{\left(2-M_t^2\sin^2\varphi\right)^2\sqrt{1-M_l^2\sin^2\varphi}+4\left(1-M_l^2\sin^2\varphi\right)\sqrt{1-M_t^2\sin^2\varphi}}{T(\varphi)} \tag{58}$$

The symbols introduced in these equations which have not been previously employed are:

$$k^2 = \frac{2M_t^2}{3 - M_t^2}$$

$$\kappa = \frac{1}{k}$$

$$\eta = \frac{2M_t^2 \sin^2\varphi}{3 - M_t^2 \sin^2\varphi}$$

$$T(\varphi) = \left(1 - \frac{1}{4} M_t^2 \sin^2\varphi\right)\left(1 - \alpha_1^2 M_t^2 \sin^2\varphi\right)\left(1 - \alpha_2^2 M_t^2 \sin^2\varphi\right)$$

$$\gamma_1 = -8$$

$$\gamma_2 = 4\left(3\sqrt{3} - 5\right)$$

$$\gamma_3 = -4\left(3\sqrt{3} + 5\right)$$

K(k) is the complete elliptic integral of the first kind, $\Pi(\alpha,k)$ is the complete elliptic integral of the third kind, H(x) is the unit step function, and sgn(x) is the sign function.

In equations (51) and (52), the terms having $\sqrt{1 - M_R^2}$ in the denominator are included only when $M_R < 1$. The term in equation (53) which has $\sqrt{M_R^2 - 1}$ in the denominator is included only when $M_R > 1$. The radicals $\sqrt{M_t^2 \sin^2\varphi - 1}$, $\sqrt{1 - M_t^2 \sin^2\varphi}$, and $\sqrt{1 - M_l^2 \sin^2\varphi}$ which occur in equations (55) to (58) are to be set equal to zero when the arguments become negative.

It is interesting to note that except for several minor changes in notation, the equations given for $u_{\bar{r}}$ are identical in form to those obtained in reference 15 in connection with a completely different half-space problem, the transient radial displacements produced at the surface of an elastic half-space by a concentrated stationary load having the form of a step function in time. Moreover, when $\varphi = 0$, the expressions given for the

vertical displacements are also identical in form to the vertical displacement equations given in reference 15.

Displacements Beneath the Line of Motion of the Load at Superseismic Speeds

The equations for the displacements produced at points situated directly beneath the line of motion of the load, that is, in the plane $y = 0$, can, of course, also be obtained as special cases of the general equations (28) to (49). The transverse displacement v is zero. At subseismic and transeismic speeds, the inplane displacements u and w can be expressed as complicated combinations of elliptic integrals and elementary functions. At superseismic speeds, however, the inplane displacements can be expressed completely in terms of elementary functions. The equations for this latter case are presented in this section. These results give some indication of the variation of the displacement pattern with depth at high speeds.

As before, it is convenient to introduce a system of polar coordinates $\bar{\rho},\psi$ in the $y = 0$ plane related to the Cartesian coordinates by $\bar{x} = \bar{\rho}\cos\psi$ and $z = \bar{\rho}\sin\psi$, as shown in figure 3. The origin is again always located at the instantaneous position of the moving load. The angle ψ is taken as zero along the positive X-axis and $+\frac{\pi}{2}$ along the positive Z-axis. The radial and tangential components of displacement are found to be:

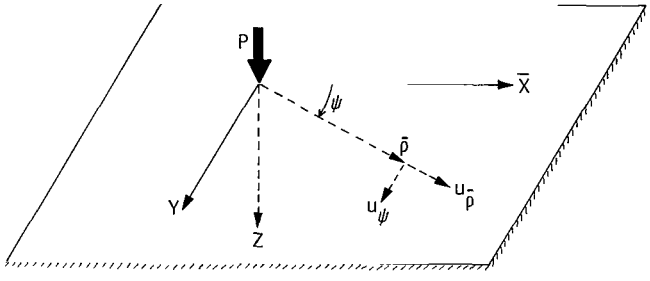

Figure 3.- Polar coordinate system $\bar{\rho},\psi$ and polar components $u_{\bar{\rho}},u_{\psi}$ of the displacements in the vertical plane $y = 0$. $\bar{\rho} = \sqrt{\bar{x}^2 + z^2}$; $\tan\psi = z/\bar{x}$.

$$\left.\begin{aligned} u_{\bar{\rho}} &= u(\bar{x},0,z)\cos\psi + w(\bar{x},0,z)\sin\psi \\ u_{\bar{\rho}} &= \frac{P'}{\bar{\rho}}\frac{3}{16\pi}H\left(\psi - \frac{\pi}{2}\right)\sin\psi\cos\psi\,N_1(\psi) \end{aligned}\right\} \tag{59}$$

and

$$\left.\begin{aligned} u_{\psi} &= w(\bar{x},0,z)\cos\psi - u(\bar{x},0,z)\sin\psi \\ u_{\psi} &= -\frac{P'}{\bar{\rho}}\frac{3\cos\psi}{32\pi M_t{}^2\sin^2\psi}H\left(\psi - \frac{\pi}{2}\right)\left[2\cos\psi\left(1 - M_t{}^2\sin^2\psi\right)N_1(\psi) + N_2(\psi)\right] \end{aligned}\right\} \tag{60}$$

where

$$N_1(\psi) = \frac{4n_t^2\cos\psi\left(\cos^2\psi - 2M_l^2\sin^2\psi\right) + \left(2\cos^2\psi - M_t^2\sin^2\psi\right)^2\sqrt{\cos^2\psi - 2M_l^2\sin^2\psi}}{\left(n_t^2 - \frac{1}{4}M_t^2\sin^2\psi\right)\left(n_t^2 - \alpha_1^2M_t^2\sin^2\psi\right)\left(n_t^2 - \alpha_2^2M_t^2\sin^2\psi\right)\sqrt{1 - M_t^2\sin^2\psi}} \tag{61}$$

$$N_2(\psi) = \frac{4n_l^2\cos\psi\left(2\cos^2\psi + M_l^2\sin^2\psi\right)\sqrt{\cos^2\psi + 2M_l^2\sin^2\psi} + \left(2\cos^2\psi + M_l^2\sin^2\psi\right)^3}{\left(n_l^2 - \frac{1}{4}M_t^2\sin^2\psi\right)\left(n_l^2 - \alpha_1^2M_t^2\sin^2\psi\right)\left(n_l^2 - \alpha_2^2M_t^2\sin^2\psi\right)\sqrt{1 - M_l^2\sin^2\psi}} \tag{62}$$

and where

$$n_t^2 = M_t^2\sin^2\psi - \cos^2\psi$$

$$n_l^2 = M_l^2\sin^2\psi - \cos^2\psi$$

The expression $N_1(\psi)$ is to be set equal to zero when the argument of $\sqrt{1 - M_t^2\sin^2\psi}$ is negative; similarly, for $N_2(\psi)$ if the argument of $\sqrt{1 - M_l^2\sin^2\psi}$ is negative. The radial component $u_{\bar{\rho}}$ is positive when the displacement is outward from the load. The tangential component u_ψ is positive when the displacement is clockwise as seen from the tip of the positive Y-axis.

Numerical Results and Discussion

Surface displacements.- Figures 4 to 10 show plots of the three components of the steady-state surface displacement for various values of M_t obtained from a numerical evaluation of equations (51) to (58). Recall that since Poisson's ratio is 1/4, the values $M_t = 0.92$, 1, and $\sqrt{3}$ correspond to load velocities equal to the speeds of the Rayleigh waves, shear waves, and compression waves, respectively. Hence, subseismic load speeds correspond to values of M_t less than unity, transeismic speeds to values of M_t between unity and $\sqrt{3}$, and superseismic speeds to M_t greater than $\sqrt{3}$.

Since all components are directly proportional to $P' = P/\mu'$ and inversely proportional to the distance from the load $\bar{r}$, it is convenient to introduce the nondimensional quantities $\bar{u}_{\bar{r}}$, $\bar{w}$, and $\bar{u}_\varphi$ defined by $u_{\bar{r}} = \frac{P'}{\bar{r}}\bar{u}_{\bar{r}}$, $w = \frac{P'}{\bar{r}}\bar{w}$, and $u_\varphi = \frac{P'}{\bar{r}}\bar{u}_\varphi$. The quantities $\bar{w}$ and $\bar{u}_\varphi$ are functions of M_t and φ only. Hence, for a fixed value of

M_t, they show the manner in which the vertical and tangential components w and u_φ vary around the load. Values of w and u_φ are shown only on the right-hand side of the line of motion of the load as seen looking in the direction of motion. The behavior of these components on the left-hand side of the line of motion can be obtained from the figures by noting from equations (51) to (58) that, with respect to this line, the vertical component is symmetric $w(-\varphi) = w(\varphi)$, and the tangential component is antisymmetric $-u_\varphi(-\varphi) = u_\varphi(\varphi)$.

Figure 4 shows the radial component of displacement over the entire speed range. Only one plot is necessary since, surprisingly enough, $\bar{u}_{\bar{r}}$ is independent of position around the load. This result is contrary to intuition which would suggest that the radial displacement ahead of a moving load might be larger than that behind the load. The radial component is inward at subseismic speeds and becomes infinite as V increases to the R-wave speed. At all other speeds $u_{\bar{r}}$ is finite and continuous. The displacement is outward at the higher transeismic speeds and decreases to zero at the P-wave speed. The radial component of displacement is zero at superseismic speeds. This result too is rather unexpected. The value of $u_{\bar{r}}$ at $M_t = 0$ corresponds to the Boussinesq solution in the special case $\lambda' = \mu'$.

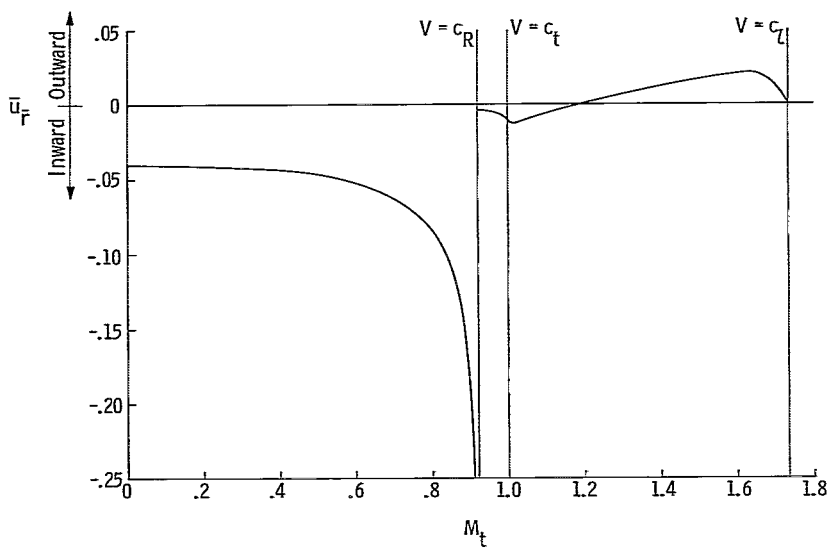

Figure 4.- Radial displacement $u_{\bar{r}} = \frac{P}{\mu' \bar{r}} \bar{u}_{\bar{r}}$ at the surface. Entire speed range. $\bar{u}_{\bar{r}} = 0$ for $c_l \leqq V$.

Figures 5 and 6 show the vertical and tangential components of displacement in the subseismic speed range. Figures 5(a) and 6(a) apply when V is less than the R-wave speed; figures 5(b) and 6(b) apply when V is between the R-wave and S-wave speeds. In addition to left-right symmetry, figure 5(a) shows that the vertical component is also symmetric fore and aft, that is, with respect to the line $\varphi = 90^o$, provided V is less than the R-wave speed. Figures 6(a) and 6(b) show that the tangential component is antisymmetric with respect to this line and zero along it at all subseismic speeds. The vertical component is seen to be considerably larger than either the radial or tangential components. The values of w and u_φ at $M_t = 0$ correspond to the Boussinesq solution for a static concentrated load when $\lambda' = \mu'$.

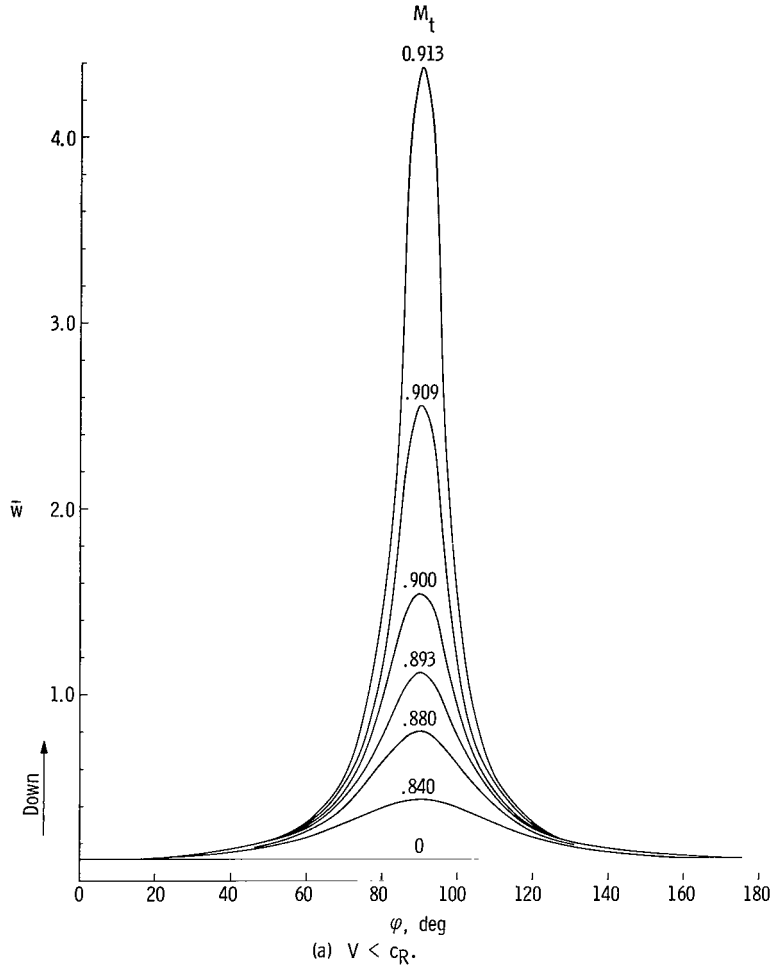

(a) $V < c_R$.

Figure 5.- Vertical displacement $w = \frac{P}{\mu' r} \bar{w}$ at the surface. Subseismic speeds.

As can be seen from figures 5(a) and 5(b), the shape of the distribution of the vertical component around the load changes abruptly as V increases through the R-wave speed. This change is due to the fact that when $V > c_R$, the load "outruns" the Rayleigh waves. A similar phenomenon, accompanied by certain changes in the displacement pattern, occurs when V increases through the S- and P-wave speeds. Some brief comments on this feature of the moving load problem seem to be in order before proceeding with a discussion of the figures.

There are three types of waves which can propagate over the surface of the solid: The R (Rayleigh) waves, S (shear) waves, and P (compression) waves. Whenever the load speed exceeds the speed of one of these waves, the effect of the corresponding waves is confined to the region of the solid bounded by the surface and the lower half of a trailing Mach cone whose apex is at the load position. The axis of the cone is the line of

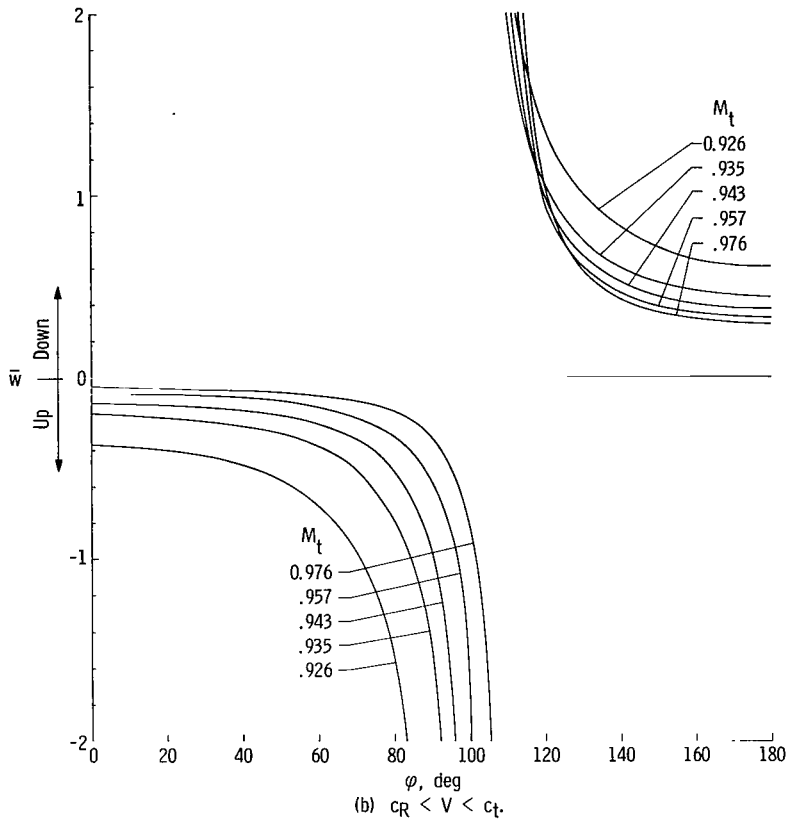

(b) $c_R < V < c_t$.

Figure 5.- Concluded.

motion and the semiapex angle is $\sin^{-1}\left(\frac{\text{Wave speed}}{\text{Load speed}}\right)$ which is equal to θ_t or θ_l when the wave speed is equal to c_t or c_l, respectively. The only region on the surface which is influenced by the waves is the trailing Mach wedge bounded by the two Mach lines $\varphi = \pm\left[\pi - \sin^{-1}\left(\frac{\text{Wave speed}}{\text{Load speed}}\right)\right]$. One Mach wedge, formed by the R-waves, occurs at subseismic speeds when $V > c_R$; two wedges, formed by the R- and S-waves, occur at transeismic speeds; and three wedges are formed at superseismic speeds. The values of φ which give the position of the pairs of trailing Mach lines for the values of M_t shown in the figures are listed for reference in table I. The symbols φ_R, φ_t, and φ_l are used for the angular positions of the Mach lines associated with the R-waves, S-waves, and P-waves, respectively. As indicated in the sketch in table I, $\varphi_l < \varphi_t < \varphi_R$.

TABLE I.- LOCATION OF MACH LINES ON THE SURFACE

Mach lines formed by
Rayleigh (R) waves ——
Shear (S) waves . . . . . .
Compression (P) waves - - - -

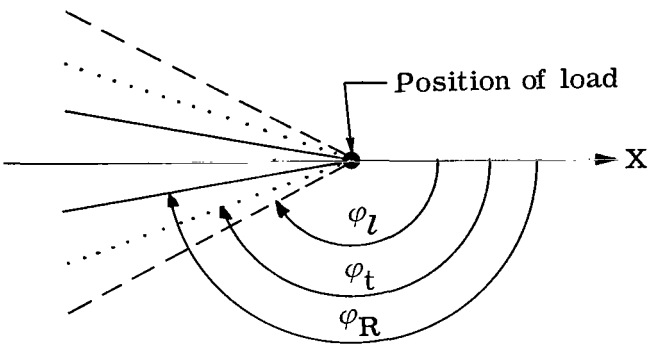

M_t	R-wave Mach lines, $\pm\varphi_R = \pi - \sin^{-1}\left(\frac{1}{M_R}\right)$, deg	S-wave Mach lines, $\pm\varphi_t = \pi - \sin^{-1}\left(\frac{1}{M_t}\right)$, deg	P-wave Mach lines, $\pm\varphi_l = \pi - \sin^{-1}\left(\frac{1}{M_l}\right)$, deg
0.919	90		
.926	97		
.935	100		
.943	103		
.957	106		
.976	110		
1.00	113	90	
1.06	119	108	
1.18	129	122	
1.33	136	131	
1.67	147	143	
$\sqrt{3}$	148	145	90
1.84	150	147	110
2.26	156	154	130
3.46	165	163	150

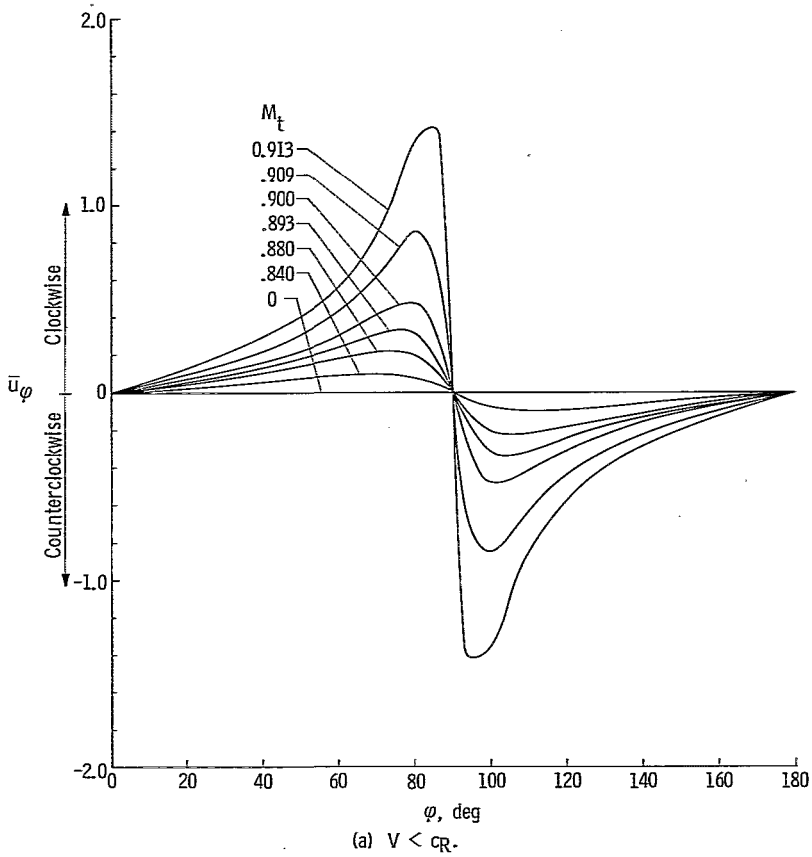

(a) $V < c_R$.

Figure 6.- Tangential displacement $u_\varphi = \frac{P}{\mu' r} \bar{u}_\varphi$ at the surface. Subseismic speeds.

In figures 5 and 6, one sees that as V increases, w and u_φ increase and become infinite at the R-wave speed. The magnitude of u_φ is very small when V is between the R-wave and S-wave speeds. The figures show that across the R-wave Mach lines, u_φ remains finite and continuous, but w experiences an infinite discontinuity and reverses its direction from up in front of the Mach lines to down behind the lines. This singularity in w across the R-wave Mach lines occurs whenever V is greater than the R-wave speed and behaves like the reciprocal of the perpendicular distance from the Mach lines. In this connection, recall that the radial component $u_{\bar{r}}$ is finite everywhere when $V > c_R$ and, like u_φ, remains continuous across the R-wave Mach lines.

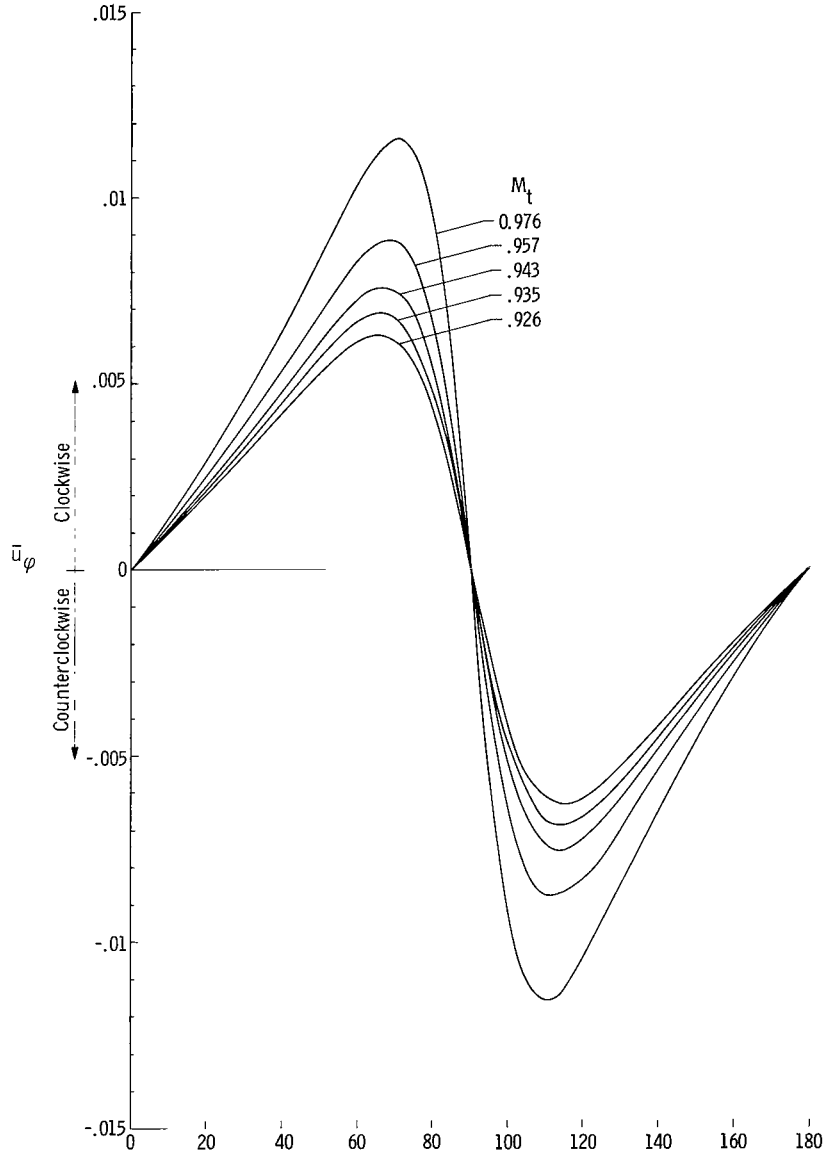

(b) $c_R < V < c_t$.

Figure 6.- Concluded.

Figures 7 and 8 show the vertical and tangential components in the transeismic speed range. The largest vertical displacements occur near the R-wave Mach lines. The direction of displacement changes from up in front of the Mach lines to down behind them. The tangential component is finite and continuous on the R-wave Mach lines but is no longer antisymmetric with respect to the line $\varphi = 90^{o}$. Both w and u_{φ} are continuous on the S-wave Mach lines but change very rapidly close to these lines. (See table I for the angular position.)

Some results at superseismic speeds are shown in figures 9 and 10. Except near the R-wave Mach lines, where w again becomes infinite and reverses direction, the vertical and tangential components are of comparable orders of magnitude. There is no disturbance ahead of the P-wave Mach lines. Both w and u_{φ} change rapidly immediately behind these lines. Figure 10 shows that the tangential component acts only in the region between the P-wave and S-wave Mach lines and is zero everywhere else. Thus, since $u_{\overline{r}}$ is also zero, there are no horizontal surface motions behind the S-wave Mach lines.

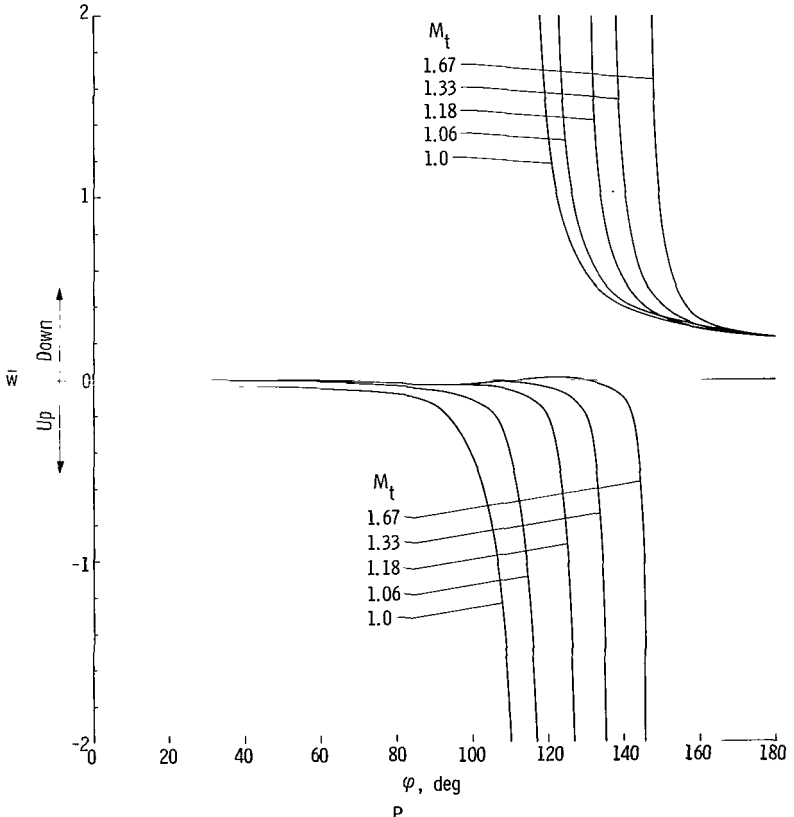

Figure 7.- Vertical displacement $w = \frac{P}{\mu' \tilde{r}} \bar{w}$ at the surface. Transeismic speeds.

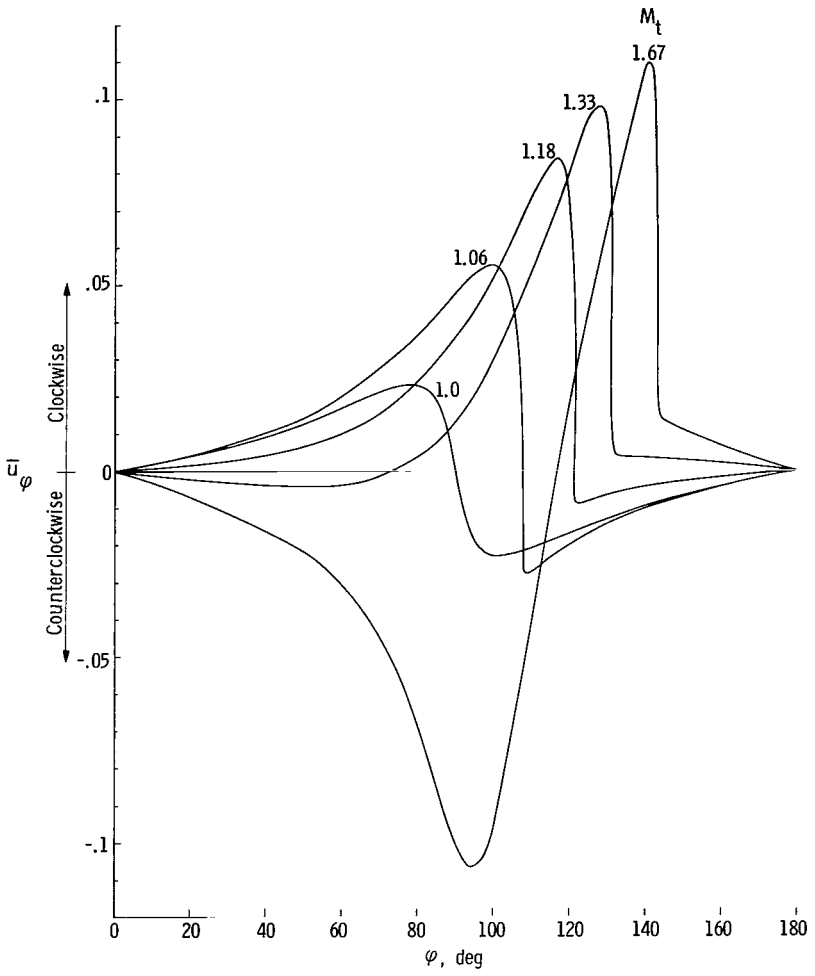

Figure 8.- Tangential displacement $u_\varphi = \frac{P}{\mu' \bar{r}} \bar{u}_\varphi$ at the surface. Transeismic speeds.

Displacements beneath the load at superseismic speeds.- The radial and tangential components of displacement in the vertical plane $y = 0$ are shown for superseismic speeds in figure 11. These components are also directly proportional to P' and inversely proportional to the distance from the load $\bar{\rho}$. For a fixed value of M_t, the functions $\bar{u}_{\bar{\rho}} = u_{\bar{\rho}} \frac{\mu' \bar{\rho}}{P}$ and $\bar{u}_\psi = u_\psi \frac{\mu' \bar{\rho}}{P}$ plotted in the figures depend only upon ψ and hence show the variation of the displacements around the load. As figure 3 indicates, $\psi = 90^o$ directly beneath the load and $\psi = 180^o$ on the surface directly behind the load. The radial and tangential components are seen to be of a comparable order of magnitude; in fact, the tangential component is larger than the radial component near the surface. Note that when $\varphi = \psi = \pi$, $u_{\bar{\rho}} = u_{\bar{r}}$ and $u_\psi = -w$. The positions of the trailing Mach lines can be determined from table I as before by simply reading ψ in place of φ. Note that there is only one Mach line in the medium associated with each wave speed.

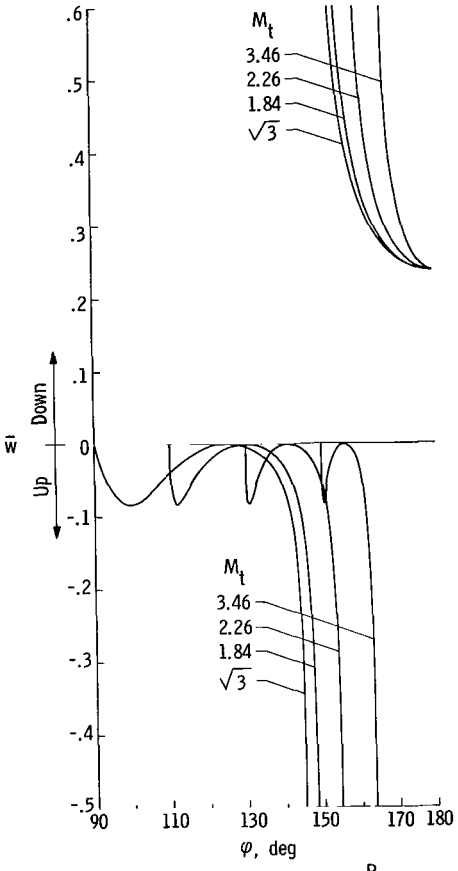

Figure 9.- Vertical displacement $w = \frac{P}{\mu' r} \bar{w}$ at the surface. Superseismic speeds.

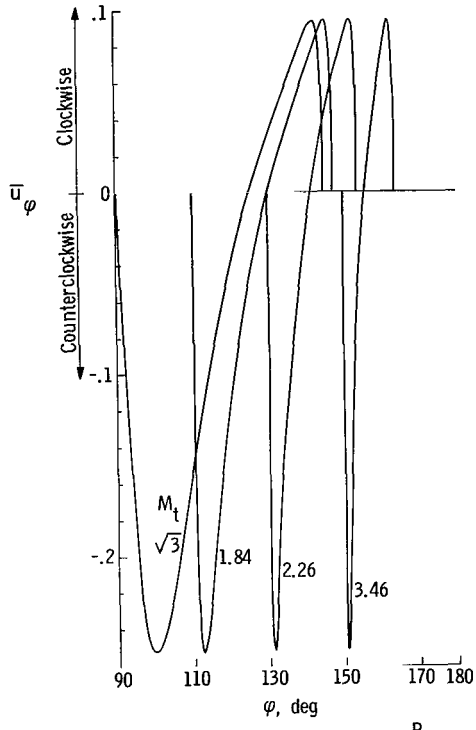

Figure 10.- Tangential displacement $u_\varphi = \frac{P}{\mu' r} \bar{u}_\varphi$ at the surface. Superseismic speeds.

Figure 11(a) shows that $u_{\overline{\rho}}$ is zero ahead of the S-wave Mach line and is infinite immediately behind this line. This singularity behaves like the reciprocal square root of the perpendicular distance from the Mach line. The radial component is continuous across the R-wave Mach line and vanishes on the surface behind the load. This result agrees with the previous results which showed that there are no horizontal surface displacements between the S-wave Mach lines. Figure 11(b) shows that the tangential component is infinite behind the P-wave Mach line. This singularity is also of the reciprocal square-root type. At the S-wave Mach line, u_ψ is continuous but has a sharp discontinuity in slope; u_ψ is also continuous across the R-wave Mach lines.

Since $u_{\overline{\rho}}$ and u_ψ are continuous across the R-wave Mach line, the vertical component of displacement $w = u_\psi \cos \psi + u_{\overline{\rho}} \sin \psi$ is also continuous there. Consequently, at least at superseismic speeds, w is not singular everywhere on the R-wave Mach cone. Since the Rayleigh wave is a surface wave, it appears probable that the infinite discontinuity in the vertical component shown in the previous figures occurs only at the surface and that w is continuous within the half-space.

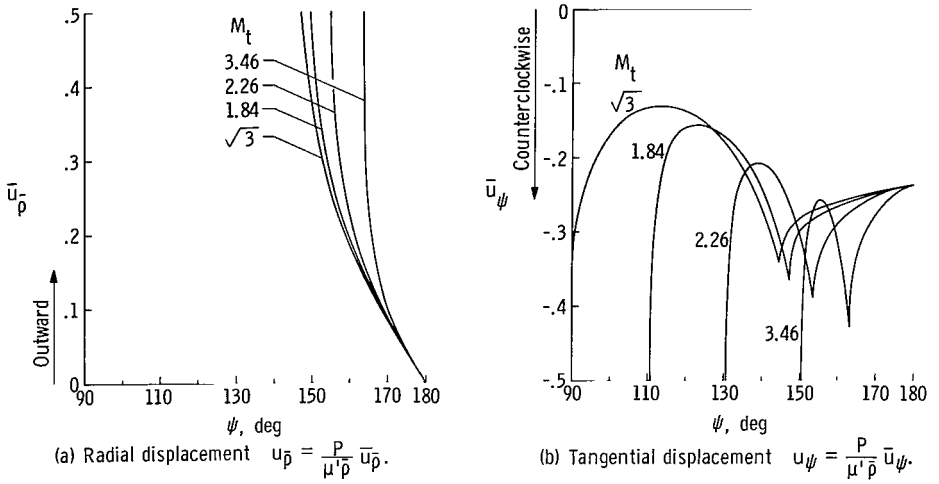

(a) Radial displacement $u_{\bar{\rho}} = \frac{P}{\mu' \bar{\rho}} \bar{u}_{\bar{\rho}}$.

(b) Tangential displacement $u_{\psi} = \frac{P}{\mu' \bar{\rho}} \bar{u}_{\psi}$.

Figure 11.- Displacements in the vertical plane $y = 0$. Superseismic speeds.

TIME-DEPENDENT HORIZONTAL SURFACE DISPLACEMENTS

At the time the moving load is first applied to the surface of the half-space, transient displacements are excited which are not accounted for in an analysis limited to the steady state. The complete time-dependent solution for the surface displacements, including these transient effects, is discussed in reference 5. In that paper the vertical displacements are obtained in closed form in terms of elementary functions over the entire speed range. The horizontal displacements, however, are very complicated. Expressions for these quantities are given in a form which is suitable for numerical calculation, but which bear no similarity to the combinations of elliptic integrals obtained in the present paper in the steady-state case. Since the steady-state solution is a limiting case of the time-dependent solution, it is reasonable to conjecture that the latter might also be expressible in terms of elliptic integrals. This conjecture was in fact found to be true.

The purpose of this section is to obtain, from physical arguments, the basic equations for determining the time-dependent horizontal components of the surface displacements and then to present for the various speed ranges expressions for these components which are comparable to the results obtained in the steady-state case. The final equations presented are valid under the assumption used previously that Poisson's ratio is 1/4. For the vertical displacements the reader is referred to reference 5.

Superposition of the Response to an Impulse

Introduce a rectangular Cartesian coordinate system X, Y, and Z fixed in the medium with the positive X-axis coincident with the line and direction of motion of the load and with the positive Z-axis pointing into the medium as shown in figure 12. This

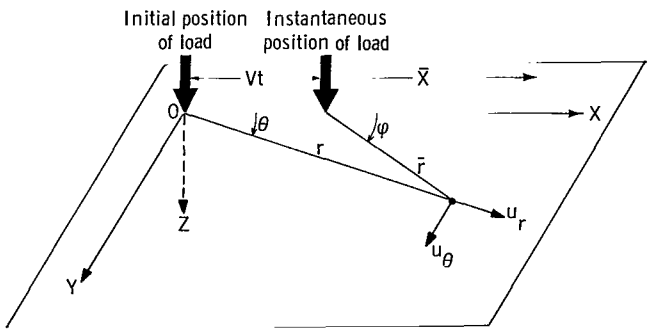

Figure 12.- Coordinate system and displacement components on the surface.

system of axes is the same as that used in the investigation of the steady-state case. Now, however, it is further assumed that the origin O of the system is located at the point on the surface at which the moving load is initially applied. Further, define $\bar{x} = x - Vt$, $\bar{r}^2 = \bar{x}^2 + y^2$, $\varphi = \tan^{-1}\frac{y}{\bar{x}}$, $r^2 = x^2 + y^2$, and $\theta = \tan^{-1}\frac{y}{x}$. The physical meaning of these variables is indicated in figure 12. The time $t = 0$ corresponds to the time at which the load is first applied to the surface. The polar coordinate system $\bar{r},\varphi$ has its origin at the instantaneous location of the moving load as before; the origin of the r,θ system is the point at which the load is initially applied. The radial and tangential components of the horizontal displacements in this latter coordinate system are denoted by u_r and u_θ, respectively.

The manner in which one can obtain the surface displacements produced by a moving load and the way in which the solution of this problem can be made to depend upon the results obtained in reference 15 is as follows: The effect of a concentrated moving load may be approximated by placing a sequence of discrete impulses along the line traveled by the load and choosing the time and location at which each impulse is to act according to the desired velocity V of the moving load. Thus, as indicated in figure 13, if the load is initially applied to the surface at point O at time $t = 0$ and the impulses are spaced at equal distance Δx apart, the first impulse is applied at time $t = 0$; the second, at time $t = \frac{\Delta x}{V}$; the third, at time $t = \frac{2\Delta x}{V}$; and so forth. The response at any point of the surface at any given time is then the sum of the responses to all the impulses which have been applied previous to that time. This approximation can be improved by increasing the number of discrete impulses until, in the limit of infinitely many impulses, the sum of the responses to the individual impulses passes over into a Duhamel superposition integral representing the response to a continuously moving concentrated load.

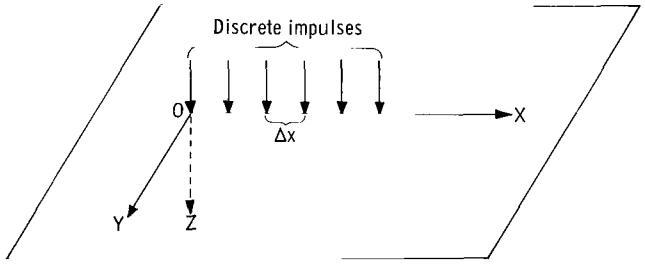

Figure 13.- Approximation of a moving load by discrete impulses. Time interval between impulses is $\Delta t = \frac{\Delta x}{V}$.

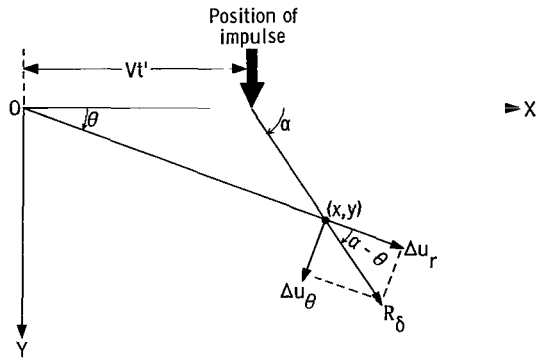

Figure 14.- Components of displacement of a single impulse. $\Delta u_r = R_\delta \cos(\alpha - \theta)$; $\Delta u_\theta = R_\delta \sin(\alpha - \theta)$.

Let $R_\delta(x - x', y - y', t - t')$ be the radial displacement produced at point x,y at time t by a unit impulse acting normal to the surface at x',y' at time t'. (By symmetry, the tangential component of displacement is zero.) Then, as shown in figure 14, the radial and tangential components $\Delta u_r, \Delta u_\theta$ of the horizontal displacement at point x,y due to a single unit impulse at $x = Vt'$, $y = 0$ are

$$\left.\begin{aligned} \Delta u_r &= R_\delta(x - Vt', y, t - t')\frac{(x - Vt')\cos\theta + y\sin\theta}{\sqrt{(x - Vt')^2 + y^2}} \\ \Delta u_\theta &= R_\delta(x - Vt', y, t - t')\frac{y\cos\theta - (x - Vt')\sin\theta}{\sqrt{(x - Vt')^2 + y^2}} \end{aligned}\right\} \tag{63}$$

If the moving concentrated load has a constant magnitude P, the strength of the approximating discrete impulses is $P\,\Delta t$. Hence, by superposition, one finds that the radial and tangential components of the horizontal displacement produced by the moving load are

$$\left.\begin{aligned} u_r &= P\int_0^t \Delta u_r\, dt' \\ u_\theta &= P\int_0^t \Delta u_\theta\, dt' \end{aligned}\right\} \tag{64}$$

These equations are combinations of the equations given in reference 5 for the Cartesian components of displacement u_x and u_y. The equations given in the reference were obtained by means of the dynamic Betti-Rayleigh reciprocal theorem rather than from physical considerations.

What is required then is an expression for the radial displacement produced by an impulse. This expression can be obtained from reference 15 which gives the expressions for the vertical and radial surface displacements produced by a stationary concentrated normal load applied to the surface as a step function in time. Since an impulse is the

time rate of change of a step function and the governing equations are linear, it follows that the response to an impulse can be obtained by differentiating the results of reference 15 for a step with respect to time. The analytical expressions for R_δ are rather involved combinations of complete elliptic integrals of the first, second, and third kinds and are not given here.

Figure 15 shows a plot of R_δ for Poisson's ratio of 1/4 as a function of the parameter $\tau = \frac{c_t t}{r}$ in which c_t is the shear wave speed, t is the time after the application of the impulse, and r is the distance of the observer from the position of the impulse. The impulse is applied in the direction of the positive Z-axis so that the surrounding surface is instantaneously in compression. The response falls off as the reciprocal of the square of the distance r. At a fixed distance, $R(\tau)$ is the time history of the radial displacement. The symbols P, S, and R denote, respectively, the times of arrival of the compression wave $\left(\tau = \frac{1}{\sqrt{3}}\right)$, shear wave ($\tau = 1$), and Rayleigh wave ($\tau = \alpha_1 \approx 1.09$) generated by the impulse. As shown in figure 15, there is no response prior to the time of arrival of the P-wave. The displacement is outward immediately after the passage of the P-wave; then it diminishes rapidly and becomes inward until about the time of arrival of the S-wave. It then increases again and becomes logarithmically infinite at $\tau = 1$. After the passage of the shear wave, the

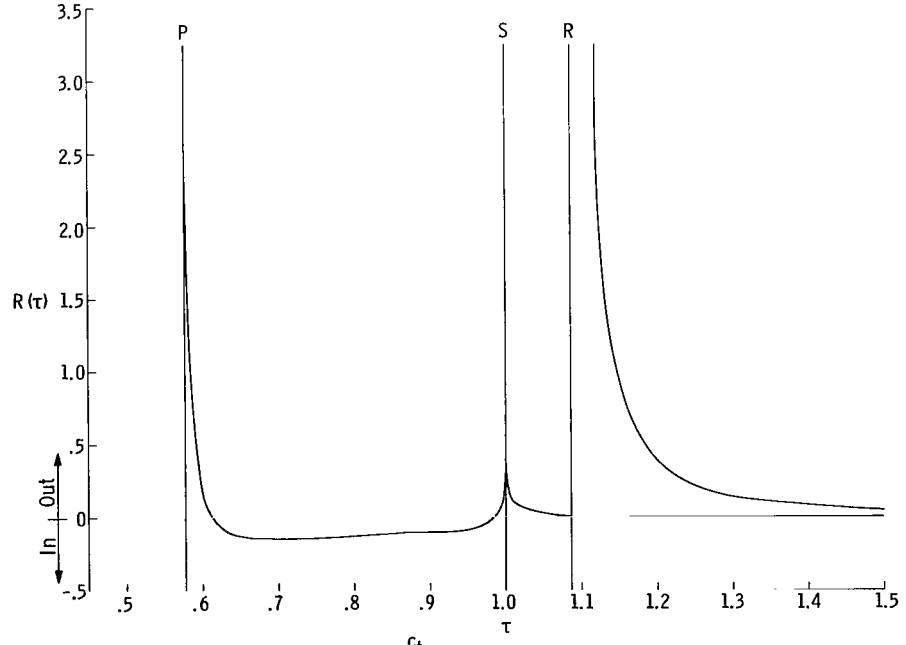

Figure 15.- Radial displacement $R_\delta = \frac{c_t}{\mu' r^2} R(\tau)$ produced at the surface by a unit impulse.

displacement rapidly decreases but remains outward. The displacement is infinite immediately after the passage of the Rayleigh wave and then steadily decreases to zero with increasing time.

Expressions for the Time-Dependent Horizontal Components of Displacement at the Surface

The results of carrying out the integrations in equations (65) are given in this section. The details are omitted; some pertinent remarks are given in the appendix in reference 5. The expressions for the time-dependent horizontal components of displacement at the surface are:

For the subseismic case; $0 < V < c_t$, $M_l < M_t < 1$:

Radial component of displacement:

$$u_r = 0 \qquad \left(\tau < \frac{1}{\sqrt{3}}\right)$$

$$u_r = \frac{P}{\mu' r} \frac{\sqrt{\frac{3}{2}}\,\tau(x\bar{x} + y^2)}{16\pi^2} \left[\frac{18}{\bar{r}^2 - \frac{1}{4} M_t{}^2 y^2} \Pi\left(\gamma_1 \kappa^2, \kappa\right) - \frac{6 - 4\sqrt{3}}{\bar{r}^2 - \alpha_1{}^2 M_t{}^2 y^2} \Pi\left(\gamma_2 \kappa^2, \kappa\right) \right.$$

$$\left. - \frac{6 + 4\sqrt{3}}{\bar{r}^2 - \alpha_2{}^2 M_t{}^2 y^2} \Pi\left(\gamma_3 \kappa^2, \kappa\right) - \frac{3\left(2\bar{r}^2 - M_t{}^2 y^2\right)\left(\bar{r}^2 - M_t{}^2 y^2\right)}{T(\bar{x}, y)} \Pi\left(\eta \kappa^2, \kappa\right) \right] \qquad \left(\frac{1}{\sqrt{3}} < \tau < 1\right)$$

$$u_r = \frac{P}{\mu' r} \frac{\sqrt{\frac{3}{2}}\,\tau k\left(x\bar{x} + y^2\right)}{16\pi^2} \left[\frac{18}{\bar{r}^2 - \frac{1}{4} M_t{}^2 y^2} \Pi\left(\gamma_1, k\right) - \frac{6 - 4\sqrt{3}}{\bar{r}^2 - \alpha_1{}^2 M_t{}^2 y^2} \Pi\left(\gamma_2, k\right) \right.$$

$$\left. - \frac{6 + 4\sqrt{3}}{\bar{r}^2 - \alpha_2{}^2 M_t{}^2 y^2} \Pi\left(\gamma_3, k\right) - \frac{3\left(2\bar{r}^2 - M_t{}^2 y^2\right)\left(\bar{r}^2 - M_t{}^2 y^2\right)}{T(\bar{x}, y)} \Pi(\eta, k) \right] \qquad \left(1 < \tau < \alpha_1\right)$$

(65)

Equation continued on next page

$$u_r = \frac{P}{\mu' r}\frac{\sqrt{\frac{3}{2}}\,\tau k\left(x\bar{x}+y^2\right)}{16\pi^2}\left[\frac{18}{\bar{r}^2-\frac{1}{4}M_t{}^2y^2}\Pi\left(\gamma_1,k\right)-\frac{6-4\sqrt{3}}{\bar{r}^2-\alpha_1{}^2M_t{}^2y^2}\Pi\left(\gamma_2,k\right)\right.$$

$$\left.-\frac{6+4\sqrt{3}}{\bar{r}^2-\alpha_2{}^2M_t{}^2y^2}\Pi\left(\gamma_3,k\right)-\frac{3\left(2\bar{r}^2-M_t{}^2y^2\right)\left(\bar{r}^2-M_t{}^2y^2\right)}{T(\bar{x},y)}\Pi(\eta,k)\right]$$

$$-\frac{P\tau}{8\pi\mu' r}\frac{x\bar{x}+y^2}{\left(\bar{r}^2-\alpha_1{}^2M_t{}^2y^2\right)\sqrt{\tau^2-\alpha_1{}^2}} \qquad \left(\alpha_1<\tau\right) \qquad (65)$$

Tangential component of displacement:

$$u_\theta = 0 \qquad \left(\tau<\frac{1}{\sqrt{3}}\right)$$

$$u_\theta = \frac{P}{\mu'}\frac{\sqrt{\frac{3}{2}}\,M_t y}{16\pi^2}\left[18\frac{\tau^2-\frac{1}{4}}{\bar{r}^2-\frac{1}{4}M_t{}^2y^2}\Pi\left(\gamma_1\kappa^2,\kappa\right)-\left(6-4\sqrt{3}\right)\frac{\tau^2-\alpha_1{}^2}{\bar{r}^2-\alpha_1{}^2M_t{}^2y^2}\Pi\left(\gamma_2\kappa^2,\kappa\right)\right.$$

$$\left.-\left(6+4\sqrt{3}\right)\frac{\tau^2-\alpha_2{}^2}{\bar{r}^2-\alpha_2{}^2M_t{}^2y^2}\Pi\left(\gamma_3\kappa^2,\kappa\right)-\frac{6K(\kappa)}{M_t{}^2y^2}+\frac{\left(x\bar{x}+y^2\right)^2}{M_t{}^2y^2r^2}\frac{3\left(2\bar{r}^2-M_t{}^2y^2\right)\left(\bar{r}^2-M_t{}^2y^2\right)}{T(\bar{x},y)}\Pi\left(\eta\kappa^2,\kappa\right)\right] \qquad \left(\frac{1}{\sqrt{3}}<\tau<1\right)$$

$$u_\theta = \frac{P}{\mu'}\frac{\sqrt{\frac{3}{2}}\,kM_t y}{16\pi^2}\left[18\frac{\tau^2-\frac{1}{4}}{\bar{r}^2-\frac{1}{4}M_t{}^2y^2}\Pi\left(\gamma_1,k\right)-\left(6-4\sqrt{3}\right)\frac{\tau^2-\alpha_1{}^2}{\bar{r}^2-\alpha_1{}^2M_t{}^2y^2}\Pi\left(\gamma_2,k\right)\right.$$

$$\left.-\left(6+4\sqrt{3}\right)\frac{\tau^2-\alpha_2{}^2}{\bar{r}^2-\alpha_2{}^2M_t{}^2y^2}\Pi\left(\gamma_3,k\right)-\frac{6K(k)}{M_t{}^2y^2}+\frac{\left(x\bar{x}+y^2\right)^2}{M_t{}^2y^2r^2}\frac{3\left(2\bar{r}^2-M_t{}^2y^2\right)\left(\bar{r}^2-M_t{}^2y^2\right)}{T(\bar{x},y)}\Pi(\eta,k)\right] \qquad \left(1<\tau<\alpha_1\right)$$

$$u_\theta = \frac{P}{\mu'}\frac{\sqrt{\frac{3}{2}}\,kM_t y}{16\pi^2}\left[18\frac{\tau^2-\frac{1}{4}}{\bar{r}^2-\frac{1}{4}M_t{}^2y^2}\Pi\left(\gamma_1,k\right)-\left(6-4\sqrt{3}\right)\frac{\tau^2-\alpha_1{}^2}{\bar{r}^2-\alpha_1{}^2M_t{}^2y^2}\Pi\left(\gamma_2,k\right)\right.$$

$$\left.-\left(6+4\sqrt{3}\right)\frac{\tau^2-\alpha_2{}^2}{\bar{r}^2-\alpha_2{}^2M_t{}^2y^2}\Pi\left(\gamma_3,k\right)-\frac{6K(k)}{M_t{}^2y^2}+\frac{\left(x\bar{x}+y^2\right)^2}{M_t{}^2y^2r^2}\frac{3\left(2\bar{r}^2-M_t{}^2y^2\right)\left(\bar{r}^2-M_t{}^2y^2\right)}{T(\bar{x},y)}\Pi(\eta,k)\right]$$

$$-\frac{PM_t y}{8\pi\mu'}\frac{\sqrt{\tau^2-\alpha_1{}^2}}{\bar{r}^2-\alpha_1{}^2M_t{}^2y^2} \qquad \left(\alpha_1<\tau\right) \qquad (66)$$

For the transeismic case; $c_t < V < c_l$, $M_l < 1 < M_t$:

Results for this case are obtained from the subseismic case by adding the following terms to the expressions for the region $1/\sqrt{3} < \tau < 1$:

To u_r, add

$$\frac{3PM_t\tau}{16\pi\mu'}|y|H\left[-(x\bar{x}+y^2)\right]\frac{\left(2\bar{r}^2 - M_t{}^2y2\right)\sqrt{\bar{r}^2 - M_l{}^2y^2}\sqrt{M_t{}^2y2 - \bar{r}^2}}{T(\bar{x},y)} \tag{67a}$$

To u_θ, add

$$-\frac{3P(x\bar{x}+y^2)}{16\pi\mu'r}\,\mathrm{sgn}(y)H\left[-(x\bar{x}+y^2)\right]\frac{\left(2\bar{r}^2 - M_t{}^2y2\right)\sqrt{\bar{r}^2 - M_l{}^2y^2}\sqrt{M_t{}^2y2 - \bar{r}^2}}{T(\bar{x},y)} \tag{67b}$$

For the superseismic case; $c_t < c_l < V$, $1 < M_l < M_t$:

Results for this case are the same as those for the transeismic case when $\tau > \frac{1}{\sqrt{3}}$.

In addition, when $\tau < \frac{1}{\sqrt{3}}$,

$$u_r = \frac{3PM_t\tau}{16\pi\mu'}|y|H(-\bar{x})\frac{\left(2\bar{r}^2 - M_t{}^2y2\right)\sqrt{\bar{r}^2 - M_l{}^2y^2}\sqrt{M_t{}^2y2 - \bar{r}^2}}{T(\bar{x},y)} \tag{68a}$$

$$u_\theta = -\frac{3P(x\bar{x}+y^2)}{16\pi\mu'r}\,H(-\bar{x})\,\mathrm{sgn}(y)\frac{\left(2\bar{r}^2 - M_t{}^2y2\right)\sqrt{\bar{r}^2 - M_l{}^2y^2}\sqrt{M_t{}^2y2 - \bar{r}^2}}{T(\bar{x},y)} \tag{68b}$$

In these equations

$$\tau = \frac{c_t t}{r}$$

$$k^2 = \frac{2}{3\tau^2 - 1}$$

$$\kappa = 1/k$$

$$\eta = \frac{2M_l{}^2y^2}{\bar{r}^2 - M_l{}^2y^2} = \frac{2M_t{}^2\sin^2\varphi}{3 - M_t{}^2\sin^2\varphi}$$

$$T(\bar{x},y) = \left(\bar{r}^2 - \frac{1}{4}M_t{}^2y^2\right)\left(\bar{r}^2 - \alpha_1{}^2M_t{}^2y^2\right)\left(\bar{r}^2 - \alpha_2{}^2M_t{}^2y^2\right)$$

$$\gamma_1 = -8$$

$$\gamma_2 = 4\left(3\sqrt{3} - 5\right)$$

$$\gamma_3 = -4\left(3\sqrt{3} + 5\right)$$

The other symbols in these equations have been defined previously. The square roots in equations (67) and (68) are to be set equal to zero when the argument becomes negative. The values $\tau = \frac{1}{\sqrt{3}}$, 1, and α_1 correspond, respectively, to the arrival times of the P-wave, S-wave, and R-wave generated at the point of application of the load. Note that when $V = 0$, equations (66) give $u_\theta = 0$, and equations (65) reduce to the result given in reference 15.

The results obtained previously for the steady-state surface displacements may be extracted from equations (66) to (69) by forming the expressions for $u_{\bar{r}}$ and u_φ, replacing x everywhere by $\bar{x} + Vt$, and then taking the limit as t approaches ∞.

Discussion of Results

The general features of the horizontal surface motions can be discussed with the aid of figure 16 which shows for comparison a sketch referring to each of the possible speed ranges. In each sketch, one is looking down upon the surface. The cross denotes the point at which the load was initially applied; the black dot indicates the position of the load. The dashed line indicates the path along which the load is moving. The concentric circles whose common center lies at the cross indicate the position on the surface of the P-, S-, and R-waves generated at the time of application of the load. The lines from the position of the load tangent to the circles are the trailing Mach lines.

In each of the four cases shown, the position of the load relative to the P-, S-, and R-waves does not change with time; for example, if $c_R < V < c_t$, the load always lies between the R- and S-waves generated at the starting position. If the moving load is thought of as a sequence of impulses, it follows that distinct P-, S-, and R-waves are

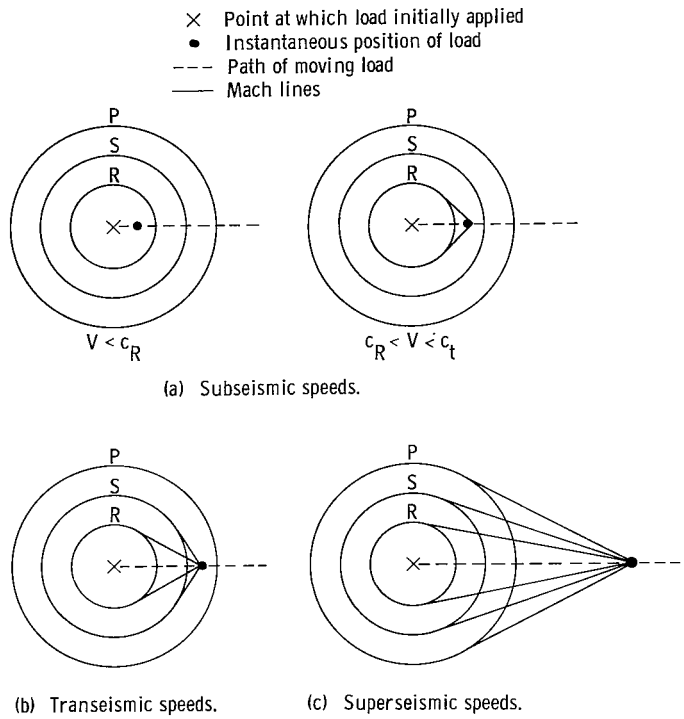

(a) Subseismic speeds.

(b) Transeismic speeds.

(c) Superseismic speeds.

Figure 16.- Waves and Mach lines associated with the surface displacements.

generated by each impulse. But in the process of superimposing the impulses, these distinct waves except those generated at the origin lose their individuality and cannot be separated from the overall pattern of displacements.

From equations (65) to (68), it follows that the radial component is symmetric and the tangential component is antisymmetric with respect to the path of the load. There is no disturbance ahead of the P-wave except in the superseismic case. Whenever the speed of the load is greater than one of the wave speeds, these waves will be confined to a wedge-shaped region between the Mach lines which trail behind the load. Three such wedges are formed in the superseismic case. It is convenient to distinguish between transient effects which tend to decay in amplitude as the load moves and steady-state effects which tend to form a fixed pattern of displacements moving over the surface at the velocity of the load. Of course, to an observer situated at a given point on the surface, the problem is completely transient in nature.

The transient effects consist of the contribution to the displacements of the P-, S-, and R-waves generated at the point of application of the load. It can be inferred from the equations that both the radial and tangential components of displacement increase after the passage of the P-wave and remain continuous across the S-wave. The tangential component is finite during the passage of the Rayleigh wave but increases rapidly behind the wave. The radial component is finite until the arrival of the Rayleigh wave. Behind

the wave it becomes infinite with the characteristic reciprocal square root singularity. After the passage of the R-wave, the disturbance dies out and eventually leaves the surface in its original undeformed state. The displacements are generally larger in magnitude in the direction of motion of the load than in the opposite direction. The amplitude of the P- and S-waves decays as $1/r$; therefore, the associated displacements are not appreciable at moderate distances from the point of application. Also the Rayleigh wave, which has infinite amplitude in theory, will be dissipated by the losses present in a real medium. But since the amplitude falls off as $\frac{1}{\sqrt{r}}$, the associated displacements should, at a given distance, be more perceptible than those associated with the P- and S-waves. For the same reason the Rayleigh wave should be noticeable at greater distances than P- and S-waves.

Superimposed upon these transient displacements there is a steady-state pattern of displacements which has a fixed distribution with respect to an observer moving with the load and which moves over the surface with the load velocity. This pattern consists of the displacements produced by the presence of the concentrated load and, whenever $V > c_R$, a system of one or more trailing Mach lines. The amplitude of the displacements in this pattern ultimately depends upon the distance from the load and not upon the distance from the initial point of application. Thus, points near the path of the load receive the full effect of the steady-state pattern even though they are at considerable distances from the origin.

In the steady-state pattern the displacements are proportional to $1/\sqrt{r}$ and become infinite at the position of the load. In the superseismic case there is no disturbance ahead of the trailing Mach lines formed by the compression waves. At slower speeds only some, or none, of the waves are confined behind the load; in these cases the surface is displaced prior to the arrival of the load. The horizontal displacements vary continuously through the compression and shear wave Mach lines but change very rapidly as the lines are crossed. There is no discontinuity in the horizontal displacements across the Rayleigh wave Mach lines. A fuller discussion of the steady-state displacements and some numerical calculations of their magnitudes have already been presented.

Figure 17 shows some sketches of the radial displacement along the positive X-axis shortly after the load has begun to move. These diagrams are based upon some calculations made for specific values of t, c_t, and V but are believed to be representative of the type of results to be expected in general. The sketches are not to scale as they are presented only to illustrate the gross features of the displacement pattern, in particular, the overall shape and the direction of particle motion. It is interesting to note that

except for a multiplying factor which takes into account the motion of the load, the equations for u_r when $y = 0$ are identical to those given in reference 15 for a completely different problem, the radial displacement due to a step function.

The symbols P, S, R, and L in figure 17 denote, respectively, the position of the P-wave, S-wave, R-wave, and the load. As indicated, the largest displacements occur near the location of the load and immediately behind the R-wave. Note that the infinite displacements behind the R-wave and near the load change direction as V varies. There is no radial displacement between L and P in the superseismic case.

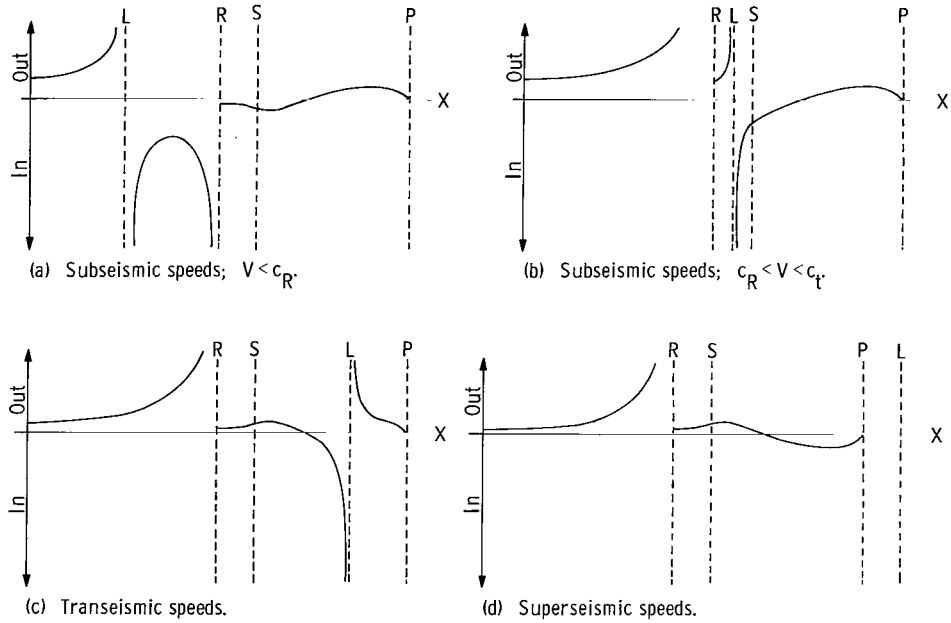

Figure 17.- Shape of radial displacements along positive X-axis.

CONCLUDING REMARKS

In this paper equations have been derived for the steady-state displacements produced within an elastic half-space by a concentrated normal load in uniform motion over the surface. The results are valid for all depths, load speeds, and elastic constants. They may be used to evaluate the subsurface stresses and strains and, in conjunction with known superposition principles, could be employed to calculate the response of the half-space to distributed surface loads.

The equations for the displacements produced on the surface at all speeds and in the vertical plane containing the line of motion of the loads at superseismic speeds have been expressed in terms of elementary functions and complete elliptic integrals in the

special case of Poisson's ratio equal to 1/4. Some numerical calculations based upon these equations have been presented and discussed for a wide range of load speeds.

On the surface it was found that the radial component of displacement was independent of the position around the load. This component is finite and continuous except at the Rayleigh wave speed (where all surface displacements become infinite) and vanishes at superseismic speeds. At subseismic speeds the tangential component is antisymmetric fore and aft and left and right of the load (quadripole distribution). At higher load speeds this component is finite and continuous across all Mach lines but changes rapidly near the compression wave (P) and shear wave (S) Mach lines. At superseismic speeds the only horizontal surface motions are tangential and these motions occur only between the P-wave and S-wave Mach lines. The vertical component predominates over the horizontal at all speeds. The most significant feature of the vertical component is the appearance of an infinite discontinuity across the Rayleigh wave Mach lines.

At superseismic speeds the radial component of displacement in the vertical plane containing the line of motion of the load vanishes everywhere ahead of the shear wave Mach lines. This component is infinite immediately behind the S-wave Mach lines and vanishes with decreasing depth. The tangential component is infinite immediately behind the P-wave Mach lines and has a sharp discontinuity in slope at the S-wave Mach lines.

In addition to these results for the steady-state problem, equations which include the transients excited by the initial application of the load have been derived for the horizontal surface displacements in the special case of Poisson's ratio equal to 1/4. These equations are in a form which is directly comparable with that obtained for the steady-state condition and from which some of the steady-state results can be rederived by a straightforward limiting process. The new features in the displacement pattern which occur in the complete transient solution are the appearance of a distinct compression, shear, and Rayleigh wave which propagate away from the point at which the load is initially applied. The disturbances carried by these waves decay according to the well-known laws governing spherical and cylindrical waves and the complete solution tends rather quickly toward the steady state.

Langley Research Center,
National Aeronautics and Space Administration,
Langley Station, Hampton, Va., November 30, 1965.

APPENDIX

INVERSION OF THE FOURIER TRANSFORM OF THE DISPLACEMENTS

The purpose of this appendix is to present in detail the steps leading from the general equations for the displacements (eqs. (24) to (26)) to the results quoted in equations (27) to (46) and to the specific forms of the Rayleigh pole terms u', v', and w' given for Poisson's ratio of 1/4 (eq. (49)). The investigation falls into two basic parts: (1) studying the singularities of the integrands for the purpose of determining how to define the values of the radicals S_l and S_t and how to integrate around the Rayleigh poles to obtain a physically meaningful result, and (2) using this knowledge to carry out some of the integrations in closed form.

Singularities in the Integrals for the Displacements

The singularities in the integrals for the displacements consist of branch points associated with the P- and S-wave speeds and poles associated with the Rayleigh wave speed. When these singularities are discussed, it is convenient to allow λ and μ to take on complex values and to view the integrals in equations (24) to (26) as repeated contour integrals in two complex planes. The location of the poles and branch points relative to the path of integration then depends upon whether one considers the λ-plane or the μ-plane. In the following, μ will be taken as a real number and the location of the singularities are treated with respect to the complex λ-plane. This choice is arbitrary; one could equally as well take λ real and study the location of the singularities in the complex μ-plane.

Rayleigh poles.- Any poles of the integrands occur at the zeros of $\Delta(\lambda,\mu)$. When $\epsilon = 0$, the equation for these zeros is

$$\left[2\left(\lambda^2 + \mu^2\right) - M_t{}^2\lambda^2\right]^2 - 4\left(\lambda^2 + \mu^2\right)\sqrt{\lambda^2 + \mu^2 - M_t{}^2\lambda^2}\sqrt{\lambda^2 + \mu^2 - M_l{}^2\lambda^2} = 0$$

After this equation is rationalized and simplified, one obtains

$$\lambda^2\left(\lambda^2 + \mu^2 - \alpha_1{}^2M_t{}^2\lambda^2\right)\left(\lambda^2 + \mu^2 - \frac{1}{4}M_t{}^2\lambda^2\right)\left(\lambda^2 + \mu^2 - \alpha_2{}^2M_t{}^2\lambda^2\right) = 0$$

where $\alpha_1{}^2 = \frac{3 + \sqrt{3}}{4}$ and $\alpha_2{}^2 = \frac{3 - \sqrt{3}}{4}$. The assumption that Poisson's ratio is 1/4 has been used so that $M_l{}^2 = \frac{1}{3}M_t{}^2$. The third and fourth factors may be disregarded as they give extraneous roots. Since the numerators in the integrals for the displacements are

of the order of λ^2 as λ approaches 0, the double root $\lambda = 0$ is associated with a removable singularity and may also be disregarded.

The factor $\lambda^2 + \mu^2 - \alpha_1^2 M_t^2 \lambda^2 = 0$ results in two simple poles which are referred to as the Rayleigh poles since if one sets $c_R = c_t/\alpha_1$, c_R is the Rayleigh wave speed if Poisson's ratio is assumed to be 1/4. For the following discussion it is convenient to define $M_R = \frac{V}{c_R} = \alpha_1 M_t$ and $\beta_R = \sqrt{M_R^2 - 1}$.

When $\epsilon > 0$, the zeros of $\Delta(\lambda, \mu)$ are determined by the more complicated equation $\left[2\left(\lambda^2 + \mu^2\right) - M_t^2 \lambda^2 - 2i\epsilon V\lambda\right]^2 - 4\left(\lambda^2 + \mu^2 - i\epsilon V\lambda\right) S_l S_t = 0$. From this equation one can easily show by direct substitution that the Rayleigh poles are now given by $\lambda^2 + \mu^2 = M_R^2 \lambda^2 + i\epsilon V\lambda$. Hence, in the complex λ-plane, the poles λ_1 and λ_2 are near the points $i\left[\frac{\pm|\mu|}{\sqrt{1 - M_R^2}} + C'\epsilon V\right]$ when $M_R < 1$ and near the points $\frac{\pm|\mu|}{\beta_R} - C'\epsilon V i$ when $M_R > 1$. In these equations C' is a positive number. In the first instance $M_R < 1$, the poles are on the imaginary axis. However, when $M_R > 1$, the poles lie below the real λ-axis for positive ϵ and V and move onto the real axis from below as ϵ approaches 0, as can be seen from figure 18. Thus, when $\epsilon = 0$ and $M_R > 1$, the path of integration along the real λ-axis must be indented to pass above the two Rayleigh poles. (Note that if V is negative and, as a result, the direction of motion of the load is reversed, the Rayleigh poles lie above the real λ-axis and the path of integration must be indented below the poles. The proper method of indentation appears to be exceedingly difficult to discover without the use of the parameter ϵ.) The contributions of the indentations around the Rayleigh poles to the displacements are discussed subsequently.

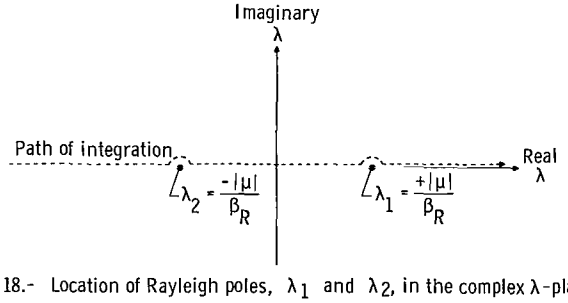

Figure 18.- Location of Rayleigh poles, λ_1 and λ_2, in the complex λ-plane when $M_R > 1$.

APPENDIX

Branch points.- Branch points occur where $S_t = 0$ and $S_l = 0$. Their location is shown to depend upon the magnitude of V relative to c_t and c_l. There are three possibilities: $V < c_t < c_l$, $c_t < V < c_l$, and $c_t < c_l < V$ which are referred to as the subseismic case, transeismic case, and superseismic case, respectively. Since the argument of each of the radicals S_t and S_l is of the form $\lambda^2 + \mu^2 - M^2\lambda^2 - iV\epsilon\lambda$ (where $M = M_t$ in S_t and $M = M_l$ in S_l), it is convenient to discuss features common to both radicals simultaneously.

The branch points occur where $\sqrt{\lambda^2 + \mu^2 - M^2\lambda^2 - iV\epsilon\lambda} = 0$. Thus, in the complex λ-plane, the branch points λ_1' and λ_2' are near the points $i\left[\pm \frac{|\mu|}{\sqrt{1 - M^2}} + c'V\epsilon\right]$ when $M < 1$ but are near the points $\pm \frac{|\mu|}{\sqrt{M^2 - 1}} - c'V\epsilon i$ when $M > 1$. In these equations c' is a positive number.

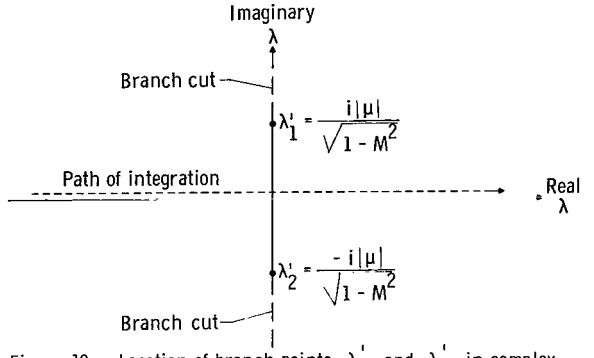

Figure 19.- Location of branch points λ_1' and λ_2' in complex λ-plane when $M < 1$.

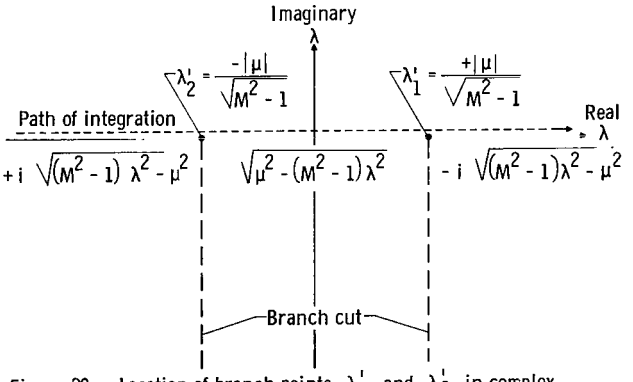

Figure 20.- Location of branch points λ_1' and λ_2' in complex λ-plane when $M > 1$.

In the first instance $M < 1$, the branch points are on the imaginary axis as shown in figure 19. The path of integration, the real λ-axis, lies between the branch points, and the branch cuts must be chosen so as to lie on opposite sides of the real λ-axis. It is convenient in this case to cut the plane along the imaginary axis from λ_1' to $+\infty i$ and from λ_2' to $-\infty i$. When $\epsilon = 0$, $\sqrt{\lambda^2 + \mu^2 - M^2\lambda^2}$ is taken as positive and and real everywhere on the path of integration.

However, when $M > 1$, both branch points lie below the real λ-axis for positive ϵ and V and, as indicated in figure 20, move onto the real axis from below as ϵ approaches 0. Now the path of integration lies above both branch points and the branch cuts must both lie in the lower half of the λ-plane. When $\epsilon = 0$, it is convenient to cut the complex

λ-plane parallel to the negative imaginary axis from λ_1' to $\lambda_1' - \infty i$ and from λ_2' to $\lambda_2' - \infty i$. The branch of the radical $\sqrt{\lambda^2 + \mu^2 - M^2\lambda^2}$ is chosen which makes the radical positive and real when $|\lambda| < \frac{|\mu|}{\sqrt{M^2 - 1}}$. The values of the radical on the path of integration between and on either side of the branch points are shown in figure 20. (Notice that if the direction of motion of the load is reversed so that V is negative, the branch points and branch cuts lie above the path of integration. The correct procedure for positioning the branch cuts is not at all clear if the parameter ϵ is omitted.)

Since the treatment of the Rayleigh poles and the branch points has been decided, the parameter ϵ has served its purpose and may be dropped. In the remaining work $\epsilon = 0$. The basic steps in reducing the double infinite integrals for the displacements (eqs. (24), (25), and (26)) to single finite integrals plus Rayleigh pole terms will now be discussed.

Reduction of the Integrals for the Displacements

The reduction of the contour integrals for the displacements is carried out in two steps. First, the contribution from the indentation of the path above the Rayleigh poles when $M_R > 1$ will be extracted from the integrals. This step still leaves integrals of the same form as those in equations (24), (25), and (26) but which must now be understood in the sense of a Cauchy principal value. By transforming these integrals from the "rectangular" coordinates λ,μ to a system of "polar" coordinates r,θ, it is found that the r-integration can be carried out explicitly and the remaining θ integrals have finite limits.

Contribution from the Rayleigh poles when $M_R > 1$.- Consider the integral $I = \int_C \frac{f(\lambda)}{\lambda - \lambda_0} d\lambda$ in which λ_0 is real and the contour C goes from $-\infty$ to $+\infty$ along the real λ-axis but avoids the pole at λ_0 by an indentation above the real axis. Then

$$I = \lim_{\eta \to 0}\left[\int_{-\infty}^{\lambda_0 - \eta} \frac{f(\lambda)}{\lambda - \lambda_0} d\lambda + \int_{C_0} \frac{f(\lambda)}{\lambda - \lambda_0} d\lambda + \int_{\lambda_0 + \eta}^{\infty} \frac{f(\lambda)}{\lambda - \lambda_0} d\lambda\right]$$

where C_0 is a semicircle of radius η above the real axis, as shown in figure 21. On the semicircle, set $\lambda = \lambda_0 + \eta e^{i\theta}$. Then

$$\lim_{\eta \to 0} \int_{C_0} \frac{f(\lambda)}{\lambda - \lambda_0} d\lambda = \lim_{\eta \to 0} \int_{\pi}^{0} f\left(\lambda_0 + \eta e^{i\theta}\right) i d\theta = -\pi i f(\lambda_0)$$

APPENDIX

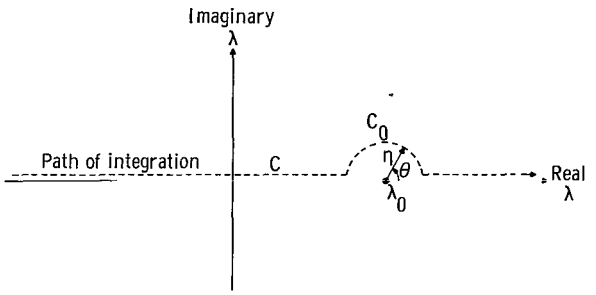

Figure 21.- Indented contour.

and

$$\lim_{\eta \to 0}\left[\int_{-\infty}^{\lambda_0-\eta} \frac{f(\lambda)}{\lambda - \lambda_0}\,d\lambda + \int_{\lambda_0+\eta}^{\infty} \frac{f(\lambda)}{\lambda - \lambda_0}\,d\lambda\right] = \oint_{-\infty}^{+\infty} \frac{f(\lambda)}{\lambda - \lambda_0}\,d\lambda$$

where the integral on the right is a Cauchy principal value. Hence

$$\int_C \frac{f(\lambda)}{\lambda - \lambda_0}\,d\lambda = -\pi i\, f(\lambda_0) + \oint_{-\infty}^{+\infty} \frac{f(\lambda)}{\lambda - \lambda_0}\,d\lambda \tag{A1}$$

By using equation (A1), the contribution from the indentation around the Rayleigh poles can be obtained as follows.

Each of the λ-integrals in equations (24), (25), and (26) is of the form $\int_C \frac{g(\lambda,\mu)}{\Delta(\lambda,\mu)}\,d\lambda$ where $\Delta(\lambda,\mu)$ has simple poles on the real λ-axis at $\lambda_1 = \frac{+|\mu|}{\beta_R}$ and $\lambda_2 = \frac{-|\mu|}{\beta_R}$ provided $M_R > 1$. In the neighborhood of the pole at $\lambda = \lambda_1$ this integral can be written as $\int_C \frac{f(\lambda)}{\lambda - \lambda_1}\,d\lambda$ where $f(\lambda) = \frac{g(\lambda,\mu)}{\frac{\Delta(\lambda,\mu)}{(\lambda - \lambda_1)}}$ and similarly, for the pole at $\lambda = \lambda_2$. Applying equation (A1) to each of the poles gives

$$\int_C \frac{g(\lambda,\mu)}{\Delta(\lambda,\mu)}\,d\lambda = -\pi i\left[\left.\frac{\frac{g(\lambda,\mu)}{\Delta(\lambda,\mu)}}{\lambda - \lambda_2}\right|_{\lambda=\lambda_2} + \left.\frac{\frac{g(\lambda,\mu)}{\Delta(\lambda,\mu)}}{\lambda - \lambda_1}\right|_{\lambda=\lambda_1}\right] + \oint_{-\infty}^{+\infty} \frac{g(\lambda,\mu)}{\Delta(\lambda,\mu)}\,d\lambda$$

$$= -\pi i\left[\frac{g(\lambda_2,\mu)}{\frac{\partial \Delta(\lambda_2,\mu)}{\partial \lambda}} + \frac{g(\lambda_1,\mu)}{\frac{\partial \Delta(\lambda_1,\mu)}{\partial \lambda}}\right] + \oint_{-\infty}^{+\infty} \frac{g(\lambda,\mu)}{\Delta(\lambda,\mu)}\,d\lambda$$

By applying this result to equations (24), (25), and (26), one finds that the expressions for the displacements become

$$(u,v,w) = (u',v',w') + (u'',v'',w'')$$

where u'', v'', and w'' are the same integrals as those which appear in equations (24), (25), and (26) but are now taken in the sense of Cauchy principal values, and the additional terms u', v', and w' arising from the Rayleigh poles are of the form

$$\int_{-\infty}^{+\infty} \left[\frac{g(\lambda_2,\mu)}{\frac{\partial \Delta(\lambda_2,\mu)}{\partial \lambda}} + \frac{g(\lambda_1,\mu)}{\frac{\partial \Delta(\lambda_1,\mu)}{\partial \lambda}} \right] d\mu$$

By substituting into this integral the appropriate values of g and carrying out the indicated integration, the expressions given in equation (49) of the text are obtained.

Transformation of the integrals for u'', v'', and w'' to polar coordinates.- The location of the branch cuts to be used in defining the value of a radical of the form $\sqrt{\lambda^2 + \mu^2 - M^2\lambda^2}$ has already been discussed. If these considerations are applied to each of the radicals S_ℓ and S_t (with $\epsilon = 0$), the system of branch cuts and the values of S_t and S_ℓ to be used in the complex λ-plane for evaluating the integrals u'', v'', and w'' are obtained. The system appropriate for each of the three speed ranges is shown in figure 22. The values of the radicals on the various portions of the real λ-axis between and beyond the branch points are also shown in the figure. The $\otimes$ marks indicate the positions of the Rayleigh poles with respect to the branch points when $M_R > 1$. To abbreviate figure 22 somewhat, it has been convenient to define $B_t = \sqrt{1 - M_t^2}$, $\beta_t = \sqrt{M_t^2 - 1}$, $B_\ell = \sqrt{1 - M_\ell^2}$, and $\beta_\ell = \sqrt{M_\ell^2 - 1}$.

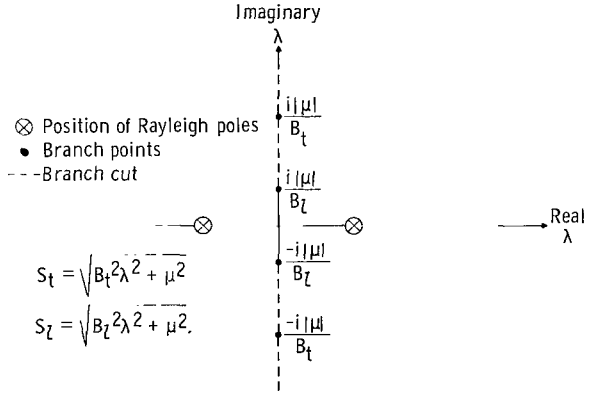

(a) Subseismic case, $V < c_t$.

Figure 22.- Position of branch cuts and values of S_ℓ and S_t on the path of integration in the three speed ranges.

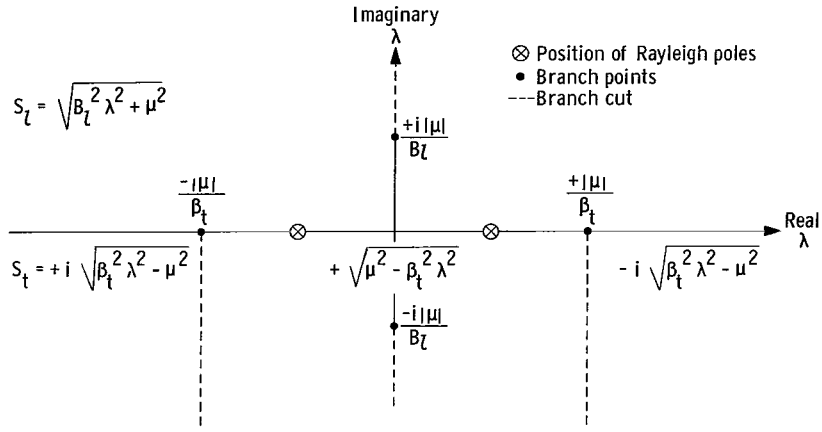

(b) Transeismic case, $c_t < V < c_l$.

Figure 22.- Continued.

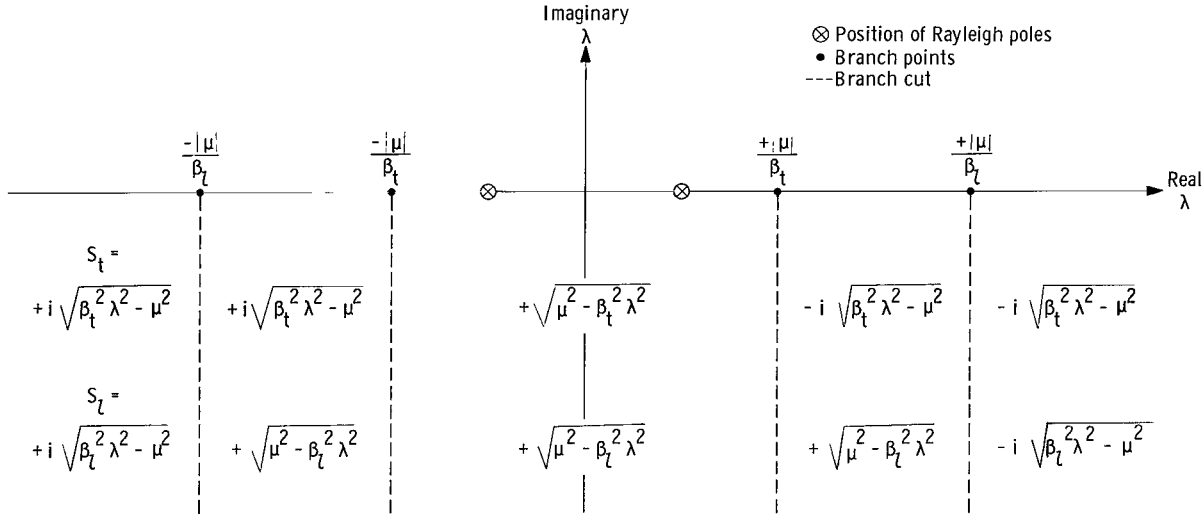

(c) Superseismic case, $c_l < V$.

Figure 22.- Concluded.

If an integral such as u'', v'', and w'' of the form $\int_{-\infty}^{+\infty}\int f(\lambda,\mu,S_t,S_l)d\lambda\, d\mu$, which so far has been treated as a repeated contour integral to be evaluated by integrating along the real λ- and μ-axes, is now viewed as a double surface integral taken over a real λ,μ plane in which λ and μ are interpreted as a system of rectangular Cartesian coordinates, the branch points on the real λ-axis in the complex λ-plane become branch "boundaries" in the Cartesian λ,μ plane and the definitions of S_l and S_t, which formerly applied to various segments of the real λ-axis, now hold over certain areas of the λ,μ plane. The value of a radical changes abruptly as one crosses a branch boundary.

Thus, for example, the imaginary branch points $\lambda = \pm i \frac{|\mu|}{B_t}$ which occur in the subseismic case have no counterpart in the real λ,μ plane. There are no branch boundaries and S_ℓ and S_t are positive and real everywhere. However, the real branch point $\lambda = + \frac{|\mu|}{\beta_t}$ which occurs in the transeismic case forms two half lines in one-half of the λ,μ plane. Similarly, the branch point $\lambda = - \frac{|\mu|}{\beta_t}$ forms two half lines in the other half of the plane. The radical S_t is real provided $|\lambda| < \frac{|\mu|}{\beta_t}$ and pure imaginary if $|\lambda| > \frac{|\mu|}{\beta_t}$. These two conditions define four regions of the λ,μ plane which are separated by the two branch boundaries $\lambda = \pm \frac{\mu}{\beta_t}$.

The result of reinterpreting figures 22(b) and 22(c) in this fashion is shown in figures 23(a) and 23(b). The subseismic case offers no difficulty and is not shown since there are no branch boundaries and S_ℓ and S_t are positive and real everywhere in the λ,μ plane. The two real branch points in the transeismic case give two branch boundaries in the λ,μ plane as shown in figure 23(a). These lines form angles $\theta_t = \sin^{-1} \frac{1}{M_t}$ with the μ-axis. The values of S_t in the four wedge-shaped regions bordered by the branch boundaries are also shown in the figure. In this case, S_ℓ is positive and real everywhere. As can be seen from figure 23(b), the four real branch points in the superseismic case give four branch boundaries in the λ,μ plane. Two of these lines are the same as those that occur in the transeismic case. The other two make angles $\theta_\ell = \sin^{-1} \frac{1}{M_\ell}$ with the μ-axis. The values of S_ℓ and S_t in the eight wedge-shaped regions of the plane bordered by the branch boundaries are also shown. Although they

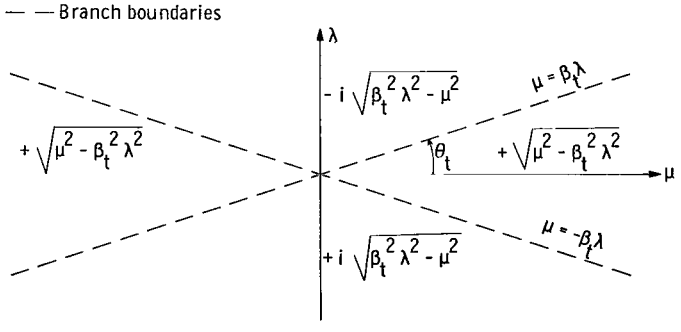

(a) Transeismic case; $S_\ell = \sqrt{B_\ell^2\lambda^2+\mu^2}$ everywhere.

Figure 23.- Position of branch boundaries and values of S_ℓ and S_t in the λ,μ plane.

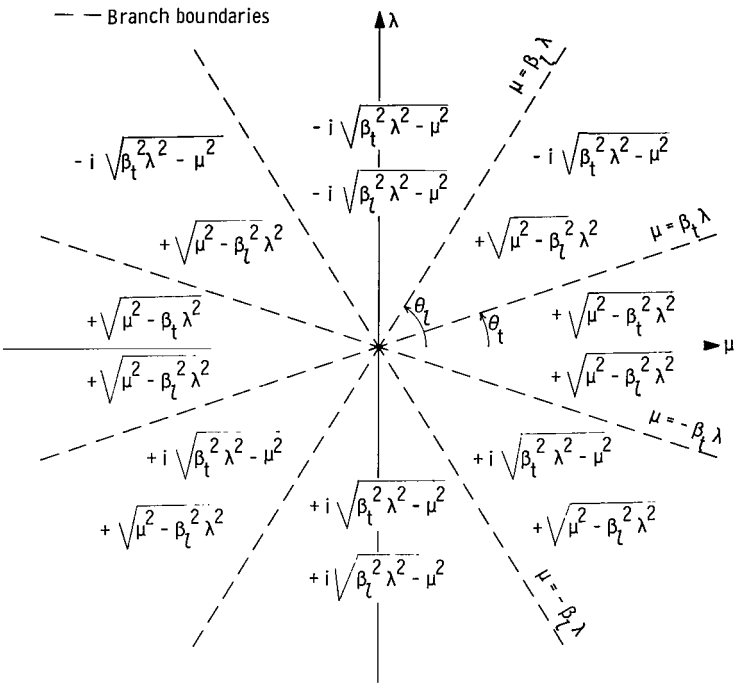

(b) Superseismic case.

Figure 23.- Concluded.

are not indicated in the figure, the Rayleigh poles also show up as two lines (when $M_R > 1$) making angles $\theta_R = \sin^{-1}\frac{1}{M_R} < \theta_t$ with the μ-axis. The integrand $f(\lambda,\mu,S_t,S_l)$ is singular everywhere along these lines; this property is signified by the Cauchy principal value. Another description of the connection between figures 22 and 23 may be of some value to the reader: figures 22(b) and 22(c) are cross sections of figures 23(a) and 23(b) along the lines μ = Constant.

Since the values of the radicals S_t and S_l have been determined throughout the λ,μ plane, the values of the integrands of the integrals for u'', v'', and w'' are also known and some progress can be made toward carrying out part of the remaining integrations in closed form. For this purpose it is convenient to transform the integrals from λ,μ coordinates to plane polar coordinates r,θ defined by $\lambda = r \sin\theta$, $\mu = r\cos\theta$. By using figure 23 as a guide, one finds that an integral of the type

$\int_{-\infty}^{+\infty}\int f(\lambda,\mu,S_t,S_l)\,d\lambda\,d\mu$ can be cast into the following form:

APPENDIX

For the subseismic case:

$$\int_0^{\infty} \oint_0^{\pi/2} f_1(r,\theta)\,d\theta\; r\; dr \tag{A2a}$$

For the transeismic case:

$$\int_0^{\infty} \left[\oint_0^{\theta_t} f_1(r,\theta)\,d\theta + \oint_{\theta_t}^{\pi/2} f_2(r,\theta)\,d\theta \right] r\; dr \tag{A2b}$$

For the superseismic case:

$$\int_0^{\infty} \left[\int_0^{\theta_t} f_1(r,\theta)\,d\theta + \int_{\theta_t}^{\theta_l} f_2(r,\theta)\,d\theta + \int_{\theta_l}^{\pi/2} f_3(r,\theta)\,d\theta \right] r\; dr \tag{A2c}$$

in which

$$\left.\begin{aligned}
f_1(r,\theta) &= f\left(r\sin\theta, r\cos\theta, r\sqrt{1 - M_t^2\sin^2\theta}, r\sqrt{1 - M_l^2\sin^2\theta}\right) \\
&\quad + f\left(r\sin\theta, -r\cos\theta, r\sqrt{1 - M_t^2\sin^2\theta}, r\sqrt{1 - M_l^2\sin^2\theta}\right) \\
&\quad + f\left(-r\sin\theta, -r\cos\theta, r\sqrt{1 - M_t^2\sin^2\theta}, r\sqrt{1 - M_l^2\sin^2\theta}\right) \\
&\quad + f\left(-r\sin\theta, r\cos\theta, r\sqrt{1 - M_t^2\sin^2\theta}, r\sqrt{1 - M_l^2\sin^2\theta}\right) \\
f_2(r,\theta) &= f\left(r\sin\theta, r\cos\theta, -ir\sqrt{M_t^2\sin^2\theta - 1}, r\sqrt{1 - M_l^2\sin^2\theta}\right) \\
&\quad + f\left(r\sin\theta, -r\cos\theta, -ir\sqrt{M_t^2\sin^2\theta - 1}, r\sqrt{1 - M_l^2\sin^2\theta}\right) \\
&\quad + f\left(-r\sin\theta, -r\cos\theta, +ir\sqrt{M_t^2\sin^2\theta - 1}, r\sqrt{1 - M_l^2\sin^2\theta}\right) \\
&\quad + f\left(-r\sin\theta, +r\cos\theta, +ir\sqrt{M_t^2\sin^2\theta - 1}, r\sqrt{1 - M_l^2\sin^2\theta}\right) \\
f_3(r,\theta) &= f\left(r\sin\theta, r\cos\theta, -ir\sqrt{M_t^2\sin^2\theta - 1}, -ir\sqrt{M_l^2\sin^2\theta - 1}\right) \\
&\quad + f\left(r\sin\theta, -r\cos\theta, -ir\sqrt{M_t^2\sin^2\theta - 1}, -ir\sqrt{M_l^2\sin^2\theta - 1}\right) \\
&\quad + f\left(-r\sin\theta, -r\cos\theta, +ir\sqrt{M_t^2\sin^2\theta - 1}, +ir\sqrt{M_l^2\sin^2\theta - 1}\right) \\
&\quad + f\left(-r\sin\theta, r\cos\theta, +ir\sqrt{M_t^2\sin^2\theta - 1}, +ir\sqrt{M_l^2\sin^2\theta - 1}\right)
\end{aligned}\right\} \tag{A3}$$

APPENDIX

Equations (A2) and (A3) are the basic formulas for reducing the integrals for u'', v'', and w'', to single finite integrals. If these formulas are applied to equations (24), (25), and (26), it is found that the r-integration can be carried out explicitly and the results can be expressed in terms of the combinations of elementary functions defined in equation (47). The final results are given in equations (28) to (47) of the text. Note that in deriving these equations there is no need to assume any specific relation between the wave speeds c_l and c_t or the Lamé constants λ' and μ'.

REFERENCES

1. Sneddon, Ian N.: Stress Produced by a Pulse of Pressure Moving Along the Surface of a Semi-Infinite Solid. Rend. Circolo Mat. Palermo, vol. 2, no. 3, Jan.-Apr. 1954, pp. 115-129.

2. Cole, J.; and Huth, J.: Stresses Produced in a Half Plane by Moving Loads. J. Appl. Mech., vol. 25, no. 4, Dec. 1958, pp. 433-436.

3. Ang, Dang Dinh: Transient Motion of a Line Load on the Surface of an Elastic Half-Space. Quart. Appl. Math., vol. XVIII, no. 3, Oct. 1960, pp. 251-256.

4. Mandel, Jean; and Avramesco, André: Déplacements Produits par une Charge Mobile á la Surface d'un Semi-Espace Élastique. Compt. Rend., vol. 252, pt. 3, May-June 1961, pp. 3730-3735.

5. Payton, R. G.: An Application of the Dynamic Betti-Rayleigh Reciprocal Theorem to Moving-Point Loads in Elastic Media. Quart. Appl. Math., vol. XXI, no. 4, Jan. 1964, pp. 299-313.

6. Love, A. E. H.: A Treatise on the Mathematical Theory of Elasticity. Fourth ed. (First Am. Printing), Dover Publ., 1944.

7. Lamb, Horace: On the Propagation of Tremors Over the Surface of an Elastic Solid. Phil. Trans. Roy. Soc. London, ser. A, vol. CCIII, no. 1, June 1, 1904, pp. 1-42.

8. Sommerfeld, Arnold: Partial Differential Equations in Physics. Academic Press, Inc., 1949.

9. Noble, B.: Methods Based on the Wiener-Hopf Technique for the Solution of Partial Differential Equations. Pergamon Press, Inc., c.1958.

10. Sneddon, Ian N.: Fourier Transforms. First ed., McGraw-Hill Book Co., Inc., 1951.

11. Van der Pol, Balth.; and Bremmer, H.: Operational Calculus Based on the Two-Sided Laplace Integral. Cambridge Univ. Press, 1950.

12. Chao, C. C.; Bleich, H. H.; and Sackman, J.: Surface Waves in an Elastic Half-Space. Trans. ASME, Ser. E.: J. Appl. Mech. (Brief Notes), vol. 28, no. 2, June 1961, pp. 300-301.

13. Baron, Melvin L.; and Lecht, Charles: Elastic Rayleigh Wave Effects Due to Nuclear Blasts. Paper No. 3346, Trans. Am. Soc. Civil Engr., vol. 127, pt. 1, 1962, pp. 802-822.

14. Byrd, Paul F.; and Friedman, Morris D.: Handbook of Elliptic Integrals for Engineers and Physicists. Lange, Maxwell & Springer, Ltd. (New York), 1954.

15. Pekeris, C. L.: The Seismic Buried Pulse. Proc. Natl. Acad. Sci. U.S., vol. 41, no. 9, Sept. 1955, pp. 629-639.

NASA-Langley, 1966 L-4470

"The aeronautical and space activities of the United States shall be conducted so as to contribute . . . to the expansion of human knowledge of phenomena in the atmosphere and space. The Administration shall provide for the widest practicable and appropriate dissemination of information concerning its activities and the results thereof."

—NATIONAL AERONAUTICS AND SPACE ACT OF 1958

NASA SCIENTIFIC AND TECHNICAL PUBLICATIONS

TECHNICAL REPORTS: Scientific and technical information considered important, complete, and a lasting contribution to existing knowledge.

TECHNICAL NOTES: Information less broad in scope but nevertheless of importance as a contribution to existing knowledge.

TECHNICAL MEMORANDUMS: Information receiving limited distribution because of preliminary data, security classification, or other reasons.

CONTRACTOR REPORTS: Technical information generated in connection with a NASA contract or grant and released under NASA auspices.

TECHNICAL TRANSLATIONS: Information published in a foreign language considered to merit NASA distribution in English.

TECHNICAL REPRINTS: Information derived from NASA activities and initially published in the form of journal articles.

SPECIAL PUBLICATIONS: Information derived from or of value to NASA activities but not necessarily reporting the results of individual NASA-programmed scientific efforts. Publications include conference proceedings, monographs, data compilations, handbooks, sourcebooks, and special bibliographies.

Details on the availability of these publications may be obtained from:

SCIENTIFIC AND TECHNICAL INFORMATION DIVISION

NATIONAL AERONAUTICS AND SPACE ADMINISTRATION

Washington, D.C. 20546